THE UNIVERSITY OF ALBERTA

A STUDY OF OROGRAPHICALLY-INDUCED VERTICAL VELOCITY

AND PRECIPITATION IN WESTERN CANADA

BY

© RONALD F. HOPKINSON

A THESIS

SUBMITTED TO THE FACULTY OF GRADUATE STUDIES AND RESEARCH

IN PARTIAL FULFILMENT OF THE REQUIREMENTS FOR THE DEGREE

OF MASTER OF SCIENCE

DEPARTMENT OF GEOGRAPHY

EDMONTON, ALBERTA

FALL, 1972

THE UNIVERSITY OF ALBERTA

FACULTY OF GRADUATE STUDIES AND RESEARCH

The undersigned certify that they have read, and recommend to the Faculty of Graduate Studies and Research, for acceptance, a thesis entitled "A Study of Orographically-Induced Vertical Velocity and Precipitation in Western Canada", submitted by Ronald F. Hopkinson in partial fulfilment of the requirements for the degree of Master of Science.

ABSTRACT

Vertical motion resulting from forced ascent or descent over sloping terrain is the primary concern of this investigation. In addition, a method of computing precipitation is adapted to estimate the contribution made to the total precipitation by the terrain-induced vertical velocities. In mountainous regions it is assumed that horizontal flow at levels above the surface is non-divergent and may be described by the stream-function. A direct method of stream-function calculation is used to yield the stream-function at the locations where the wind is measured. An objective analysis, which utilizes a continuous distance weighting scheme, extends these values to a grid oriented such that its ordinate parallels the Coastal Mountains and the Alberta Range of the Rocky Mountains in southern British Columbia and Alberta.

A scalar objective analysis is proposed to compute the horizontal velocity components relative to the grid from the more abundant reports at the earth's surface. This analysis is also used to estimate values of temperature and dewpoint temperature at the grid points from station reports. In the latter case, the analysis was applied not only to the surface, but also to the 850-mb, 700-mb and 500-mb levels where station density allows only a first approximation.

The terrain-induced vertical velocity is calculated from the equation:

$$w = V_h \cdot \nabla_h H \quad ,$$

where V_h is the horizontal wind and $\nabla_h H$, the slope of the terrain is decreased linearly with height to zero at 3 km above the terrain.

The orographic precipitation is computed using the vertical velocity, temperature and dewpoint temperature fields at a number of levels and compared to surface measurements of precipitation.

ACKNOWLEDGEMENTS

I wish to express my gratitude to a number of people who have aided in the completion of this thesis.

In particular, I am very appreciative of the advice and guidance of my departmental supervisor, Dr. E. R. Reinelt. I would also like to thank Professor R. W. Longley and Dr. R. Kellerhals for their willingness to serve on the examining committee.

I am also indebted to Mr. C. O. Charette for providing not only the inspiration for this study, but also the extracted terrain heights and a computer listing of his working model.

I am thankful to my wife, Margaret, who aided in the data extraction from synoptic maps and plotted the many grid point maps for analysis.

To Mrs. M. Calvert who typed the first and final drafts of this thesis, I am grateful. I appreciate the assistance of Mrs. Laura Smith with insertion of the Greek symbols. The advice and assistance of the technical staff of the Department of Geography during the preparation of the figures was invaluable. Mr. J. Chesterman provided the photographic reduction of many of the figures.

This study was undertaken while I was on leave from the Atmospheric Environment Service of the Department of the Environment.

TABLE OF CONTENTS

LIST OF FIGURES

CHAPTER 1

INTRODUCTION

All extensive mountain systems around the world influence
weather from the planetary scale down to the microscale. The inter-
actions between topography and the atmosphere are exceedingly complex;
attempts to study these relationships have met with varying degrees of
success, but as yet a complete understanding is lacking. Part of the
problem arises from the overlap of the various meteorological scales.
In general the terrain may be highly irregular, resulting in rapid
changes of forces exerted on a particular parcel of air. Also to be
considered are the overall orientation of the flow with respect to the
obstruction, the stability of the air mass, vertical and horizontal
wind shear, and moisture content to name only a few.

An evaluation by Newton (1971) of the torques exerted by large
mountain ranges on the atmosphere suggests that this factor may be com-
parable to surface friction in the balance of global angular momentum.
On the synoptic scale, Pettersen (1956a) in a study of cyclogenesis over
the Northern Hemisphere noted that the lee of extensive mountain
barriers was a major area for the formation of lows. A more recent
study of this same phenomenon by Chung (1972) considered the area to the
lee of the Canadian Rocky Mountains. By reducing the size of his samp-
ling squares, Chung found two additional major centres of cyclogenesis
that were not revealed by Pettersen's investigation. The last example

is typical of the problem confronting meteorologists. A further re-
duction of the mesh size would in all probability reveal an even more
involved pattern, if data were available.

McClain (1960) found that descending motion to the lee of the
Western Cordillera of North America was not in itself sufficient to
generate major cyclonic storms but, when coupled with other factors,
could result in rapid and dramatic development. Katabatic winds, moun-
tain waves and other mesoscale phenomena usually attributed to the
proximity of marked relief are also of great importance but influence a
much smaller area.

One of the most generally known aspects of mountain meteor-
ology is the enhancement of precipitation along the windward slope of
any orographic obstacle. Sawyer (1956) gives a brief but comprehensive
summary of the problems involved in estimating orographic precipitation
from physical and dynamical principles. Reinelt (1970) points out that
while in some cases the rain shadow effect may predominate, a change in
the circulation pattern will make the same area subject to terrain-
induced rain.

The present study was based on the idea that air encountering
a large mountain range will be forced to ascend the windward slope and
descend on the lee. A model proposed by Charette (1971) to calculate
the terrain-induced vertical velocities at the 850-millibar level was
modified so that less input data were required. This allowed his
approach to be extended to higher levels where the density of data dec-
reased rapidly.

Chapter 2 contains a description of the grid and the vertical
velocity calculation. The method of determining the horizontal wind

field at discrete grid points is outlined in Chapter 3. A quantitative precipitation scheme for evaluating the vertical velocities computed by the model is given in Chapter 4. The results of the calculations are presented in Chapter 5.

CHAPTER 2

OROGRAPHICALLY-INDUCED VERTICAL VELOCITIES

2.1 Introduction

McClain (1960) observed that the Western Cordillera of North
America constitutes an essentially continuous barrier from 25°N to
60°N for air below 1300 to 1500 meters. The 850-mb level is usually
found near the upper limit of this barrier and must therefore reflect
its influence. When presented with so great a north-south extent, most
of the air below 1300 meters must surmount the obstacle and descend on
the lee slope. The method used to calculate the resultant vertical
motions was based on Charette's (1971) study. Some modifications were
made to the general procedure and these are described in the following
sections.

2.2 The Grid

Charette extracted terrain heights at discrete points from
topographic maps of scale 1:250,000. These maps were part of the top-
ographic series produced and printed in Canada by the Surveys and
Mapping Branch, Department of Energy, Mines and Resources, Government
of Canada and in the United States by the Interior Geological Survey,
Washington, D.C.. The location of these points was a function of a
polar stereographic projection true at 60°N. A brief description of the
equations relating a point on the earth's surface to its projection onto
some image plane is given by Saucier (1955) and in more detail for the

particular case of a polar stereographic secant projection by Charette (1971).

The relation may be determined from:

$$r = a(1 + \cos(\theta_0))(\tan(\frac{\theta}{2})) \qquad (2\text{-}1)$$

$$\sigma = \frac{(1 + \cos(\theta_0))}{(1 + \cos(\theta))} = \frac{(1 + \sin(\phi_0))}{(1 + \sin(\phi))} \qquad (2\text{-}2)$$

where

r = radius of a latitude circle on the polar stereographic projection

a = mean radius of the earth

ϕ_0 = standard latitude, in this case 60°N

ϕ = latitude of point in question

θ_0 = $\pi/2 - \phi_0$

θ = $\pi/2 - \phi$

σ = image scale which gives the distortion of distances introduced at the latitude ϕ by the representation of the earth's surface on a polar stereographic projection with standard latitude ϕ_0.

Only equation (2-1) is required to compute the location of the grid points. The grid most commonly used by numerical weather prediction models has a grid length of 381 kilometers at 60°N on a polar stereographic projection. This grid size remains constant on the projection but the actual distances between grid points varies according to the image scale σ. In this investigation a grid length equal to one-eighth of 381 kilometers was chosen as this was the same used by Charette in the extraction of terrain heights. The ordinate of the grid was aligned with longitude 80°W.
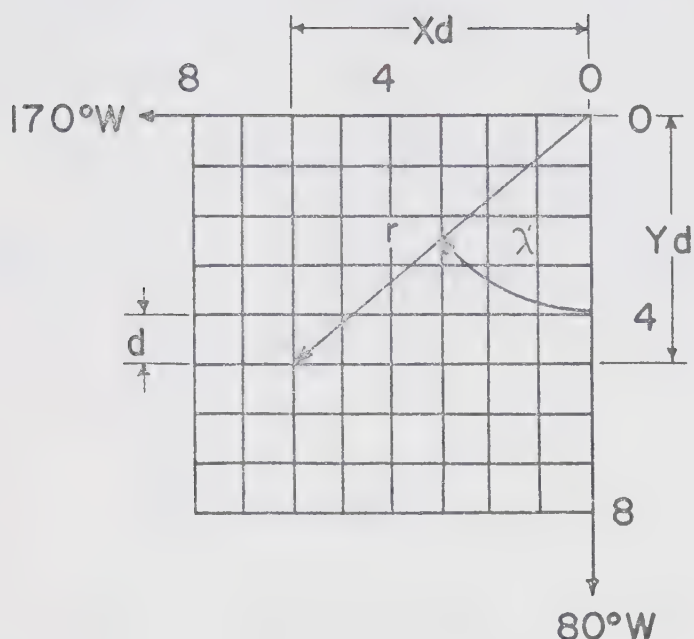
FIGURE (2-1) Calculation of the grid point coordinates from a polar stereographic secant projection at 60°N.

As illustrated in Figure (2-1) the distance r from the pole to a grid point on the projection plane may be computed in terms of one-eighth grid length[1] intervals.

$$r = \left[(Xd)^2 + (Yd)^2 \right]^{1/2}$$

where d is the grid length or

$$r = d\left[X^2 + Y^2 \right]^{1/2} \qquad (2-3)$$

Note that X and Y represent the number of grid lengths along the abscissa and ordinate, respectively. Values of increasing Y are measured

---

[1]The one-eighth grid length will henceforth be referred to as the grid length, unless otherwise stated.

downward, and increasing X to the left. By substituting this expression
for r into equation (2-1) it is possible to solve for the latitude on
the earth's surface:

$$\phi \; = \; \frac{\pi}{2} \; - \; 2 \; \arctan \left[\frac{d(X^2 + Y^2)^{1/2}}{a(1 + \cos (\theta_o))} \right] \qquad (2\text{-}4)$$

With λ' defined as in Figure (2-1) the longitude of a gridpoint may be
determined from equation (2-5):

$$\lambda \; = \; 80^o + \lambda'$$
$$= \; 80^o + \arctan (X/Y)$$

The portion of the map used in the analysis encompassed all of
British Columbia, all of Alberta with the exception of the northeast
corner, and parts of the adjacent regions of Montana, Idaho, Washington,
Oregon, Northwest Territories, Yukon, Saskatchewan and Alaska (see
Figure (2-2)).
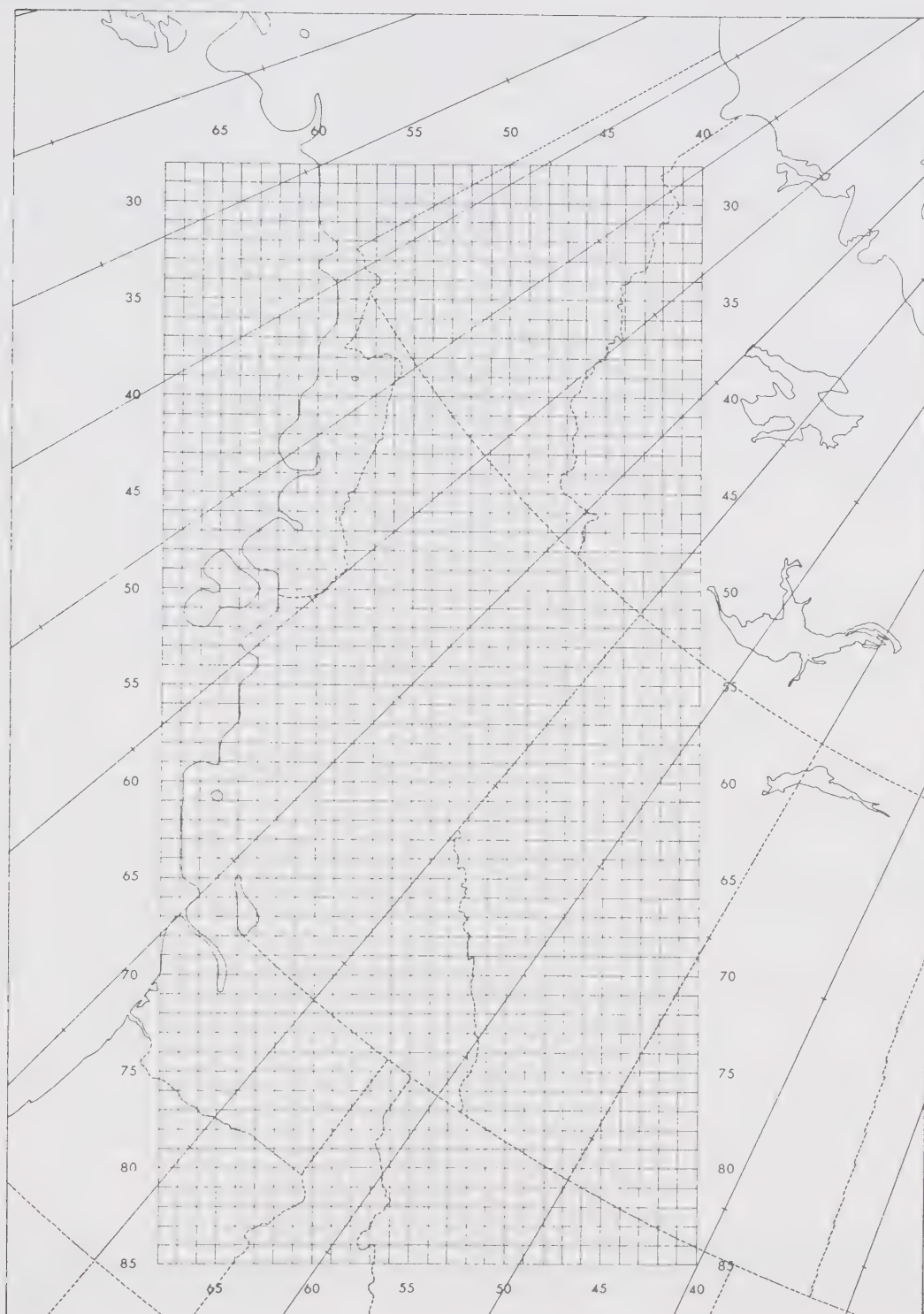
FIGURE (2-2) Grid used for orographic vertical velocity model. Numbers refer to number of grid lengths measured downward or to left of north pole. The grid is oriented such that the ordinate is parallel to 80°W longitude.

2.3 The Height Profile

Once the coordinates in latitude and longitude of each grid point were calculated the tedious but necessary extraction of heights from topographic charts was performed by Charette. He relates that, on the 1:250,000 scale, contours ranged from every 100 feet over relatively level regions to 500 feet in areas of high relief. Thus, the accuracy of the terrain heights varied as the ruggedness of the topography.

After the heights were procured he performed a smoothing operation on the data at every second grid point. The operator used is given by equation (2-6) with reference to Figure (2-3):

$$H(I,J) = \left[\frac{1}{8}(h_1 + h_2 + h_3 + h_4 + h_5 + h_6 + h_7 + h_8)\right] \times 0.6$$

$$+ h(I,J) \times 0.4 \tag{2-6}$$

O 1/4 grid points
• 1/8 grid points

1/8 grid length
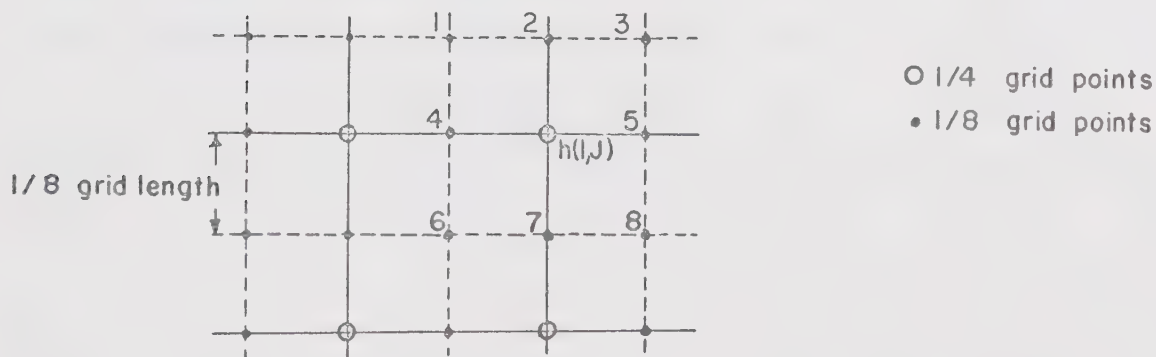
FIGURE (2-3) System of grid points used in smoothing operation. The height profile is retained at every second grid point following application of smoothing operator.

The effect of the operator combined with retention of the smoothed profile at alternate grid points provides a simplified but distorted height field. A portion of the original data field analyzed

before smoothing is shown in Figure (2-4). For comparison, the same area using the smoothed values is shown in Figure (2-5).

The reason for smoothing the field is to eliminate irregularities which, it is argued, have no bearing on the synoptic scale; however, the reduction in height of major ridges, and the associated relaxation of height gradients can be severe and excessive. In this study, it was decided, therefore, to retain the original terrain heights with the realization that a number of "unrepresentative" values might be present. This problem exists whenever any attempt is made to represent a continuous field by discrete, equally-spaced values.

The justification for not smoothing may be found in the mean value theorem from calculus. In this investigation, the important quantity was taken to be the slope of the underlying terrain. From the theorem it can be stated that at least one point between any two grid points must have a slope equal to the height gradient between the grid points, provided a first derivative exists at all the intervening positions. Therefore, the data were utilized without subsequent smoothing. The only operation performed on the data was a conversion from feet to meters. An analysis of the complete area used in the model is given in Figure (2-6). With reference to the grid shown in Figure (2-2), the analysis extends from rows 28 to 85 and columns 40 to 68 inclusive. Some distortion of shape and lack of prominent peaks results from the discrete representation, but it was felt this approach resembled reality more closely than a smoothed profile.

FIGURE (2-4) Analysis of terrain heights extracted by Charette. The
heights are labelled in thousands of feet above sea level.
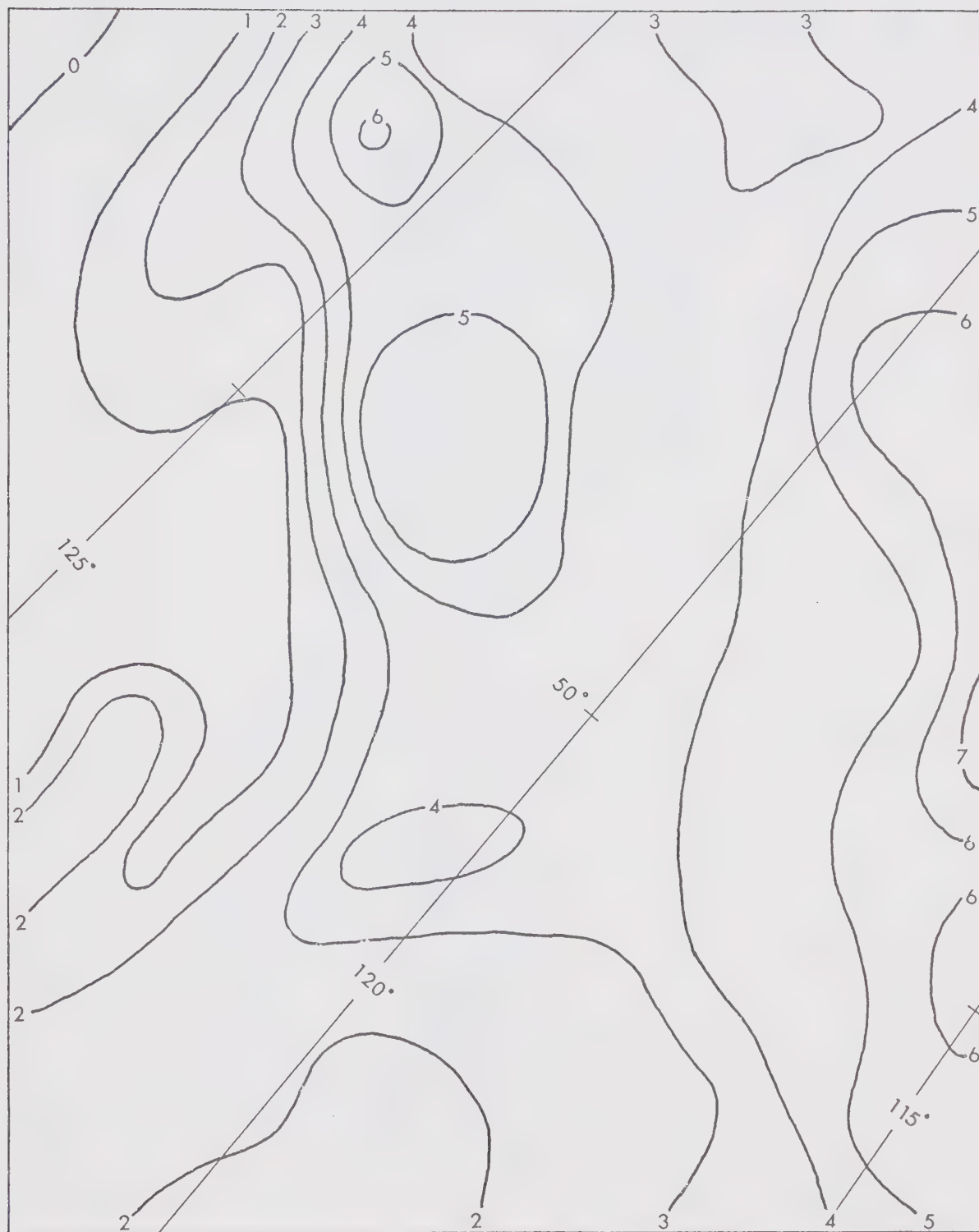
FIGURE (2-5) Analysis of smoothed terrain showing the same area as in Figure (2-4). The heights are labelled in thousands of feet above sea level.
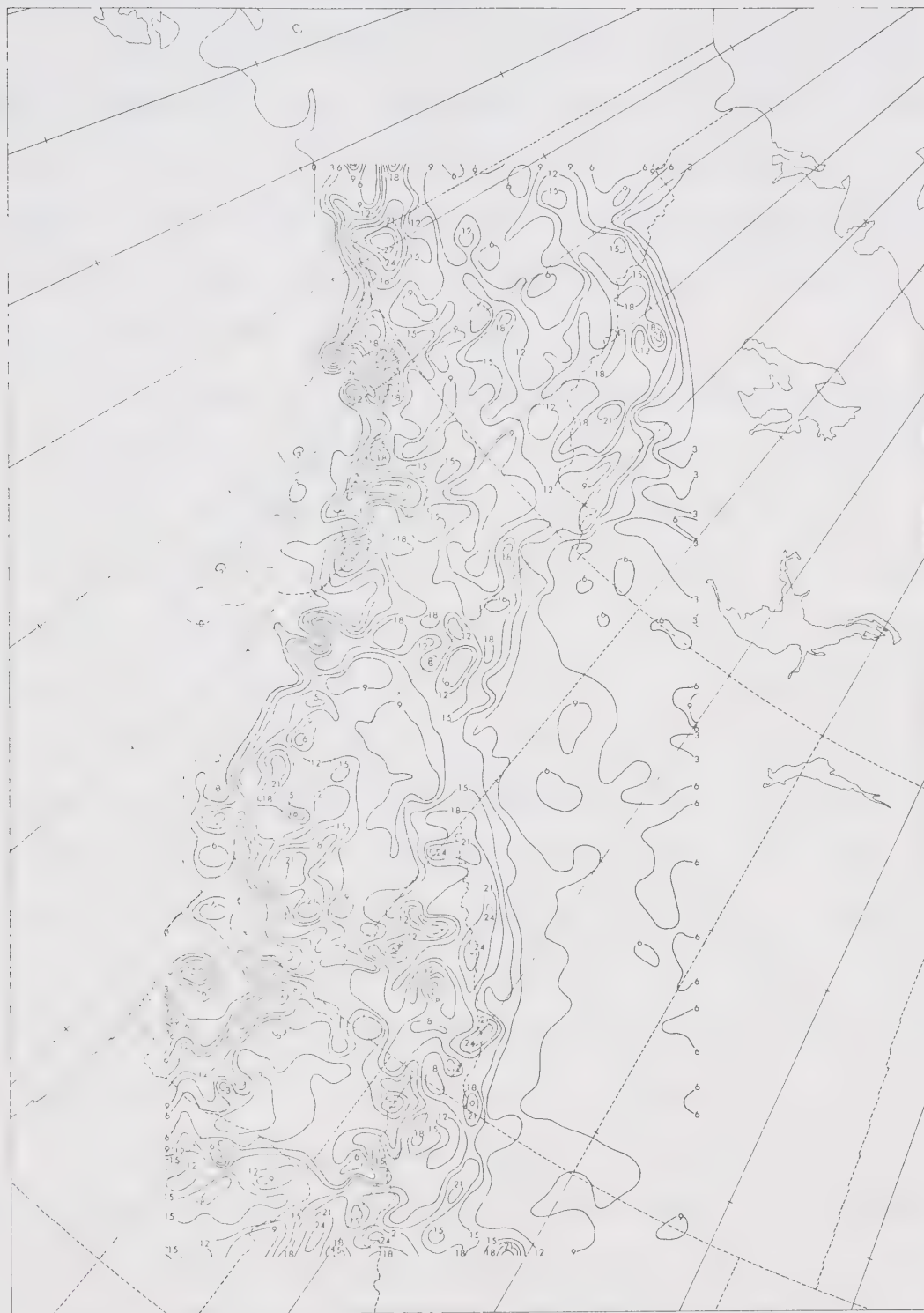
FIGURE (2-6) Height profile of that portion of the Western Cordillera
used in this model. The heights are expressed in hundreds of meters
above sea level.

2.4 The Vertical Velocity Calculation

One of the most difficult quantities to evaluate in meteor-
ology is vertical velocity. The problem stems from its small magnitude
so that it is difficult to measure directly and accurately in the free
atmosphere. Most studies of ascending or descending atmospheric motions
determine the vertical velocity indirectly from other more easily
measured parameters and theoretical principles.

Three scales of motion are commonly associated with the form-
ation of precipitation, as mentioned by Reinelt (1970). Vertical vel-
ocities of a few centimeters per second that are maintained for at
least several hours are generally attributed to synoptic systems such as
extratropical cyclones (Mason, 1962, p.9).   Near fronts this figure
may increase to 10 cm/sec, but this is considered the upper limit for
organized vertical motion over a large area. At the other end of the
scale are convective motions which may exceed 20 meters per second in
large thunderstorms, but are more usually of the order of 5 m/sec. An
individual convective cell seldom exceed a few kilometers in horizontal
extent or half an hour in duration. The third major range of vertical
velocities intermediary to the others is associated with forced ascent
or descent due to the presence of orographic obstacles.

The last case is the one studied in this investigation. Ver-
tical velocities greater than 40 cm/sec on this scale are considered
rare as this requires strong horizontal winds impinging on an extremely
steep slope. Such slopes are usually of small geographical extent, so
that it is probable that air is diverted to adjacent regions. Along a
mountain ridge, vertical motion of 5 to 15 cm/sec is more in order.
Over gently sloping terrain prolonged ascent at less than 1 cm/sec for

a fetch of hundreds or even thousands of kilometers has also been observed. Of these three situations, the second is thought to be of prime importance in the mountainous regions of the world.
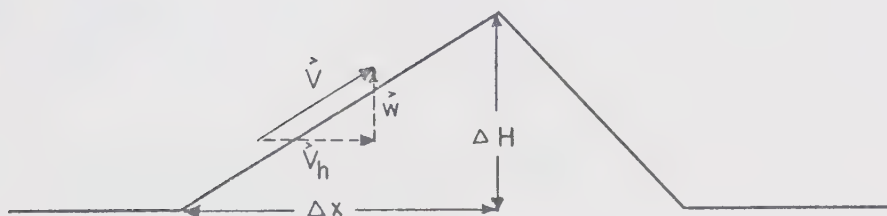
FIGURE (2-7) Cross-section of a ridge of land illustrating orographic ascent.

A parcel forced to ascend a mountain (Figure (2-7)) is assumed to follow the shape of the underlying terrain. By a method described in Chapter 3, the horizontal velocity V_h is obtained at the centre of each grid square at a number of levels. At the surface the vertical velocity was computed from equation (2-7):

$$w = \vec{V}_h \cdot \nabla_h H \qquad\qquad (2\text{-}7)$$

where w = vertical velocity component and

$$V_h = \text{horizontal wind}$$

$$\nabla_h H = \hat{i}\frac{\partial H}{\partial x} + \hat{j}\frac{\partial H}{\partial y}, \text{ the slope of the terrain. } \nabla_h H$$

was evaluated at the centre of the grid squares. The height at point A (see Figure (2-8)) was the average computed from:

$$H_A = \tfrac{1}{2}(H(I,J) + H(I + 1, J)) \qquad\qquad (2\text{-}8)$$

and, similarly, the heights at points B, C and D. In actuality this step was incorporated in the expressions for the gradients given below.

$$\frac{\partial H}{\partial x} = \frac{\sigma}{2d}\Big[H(I,J) + H(I + 1,J) - H(I, J + 1) - H(I + 1, J + 1)\Big]$$

$$(2\text{-}9)$$

$$\frac{\partial H}{\partial Y} = \frac{\sigma}{2d}\Big[H(I,J) + H(I, J + 1) - H(I + 1, J) - H(I + 1, J + 1)\Big]$$

$$(2\text{-}10)$$

where σ = image scale from equation (2-2)

$\quad$ d = grid length in meters

In component form, equation (2-7) may be written:

$$w = u\frac{\partial H}{\partial x} + v\frac{\partial H}{\partial Y} \qquad\qquad (2\text{-}11)$$
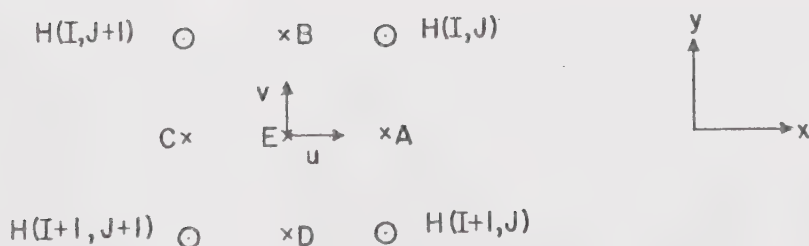
FIGURE (2-8) Evaluation of slope of terrain at point E, the centre of a grid square.

The influence of the orography was assumed to decrease with increasing height. McClain (1960) stated that no evidence existed at

that time to indicate that the synoptically important orographic motion
extended more than 3 kilometers above the terrain. While the scale
considered in this study was much smaller than synoptic, this was used
as a criterion for the upper limit of orographic vertical motion. Mountain
waves are ignored.

The exact nature of the decrease has not yet been determined
for a general case although various proposals have been made by
Smagorinsky and Collins (1955), Estoque (1957) and numerous others.
Although there was no fundamental physical reason for doing so, it was
decided to follow Charette's lead in this matter and allow the effective
slope of the topography to decrease linearly with height to zero at
3 kilometers above the terrain. Let δH represent the distance in meters
between the level under consideration and the terrain at the centre of a
grid square. Then the vertical velocity at that level due to the oro-
graphy may be expressed as:

$$ w = \vec{V}_h \cdot (1 - \frac{\delta H}{3000}) \nabla_h H \qquad (2\text{-}12) $$

In practice, the correction is applied following the calculation of w as
given in equation (2-7). The sole justification for this approach is
its simplicity, although later evaluation indicated that it was useful
as a first approximation. More elaborate methods await further invest-
igation.

The major difference between Charette's calculations and those
outlined above was the reduction of the grid length used to calculate
the slope of the topography. By centering the calculations at the middle
of the grid squares it was possible to eliminate consideration of the

wind direction when computing the gradients. Downward motion may now
be overestimated in the case of narrow valleys where air tends to stag-
nate but this was not thought to be important in the summer and autumn
situations studied.

CHAPTER 3

STREAM-FUNCTION ANALYSIS AND SCALAR OBJECTIVE ANALYSIS

3.1 Introduction

In order to proceed with the vertical velocity calculations mentioned in the previous chapter it is necessary to compute the horizontal wind components at the centre of the grid squares. Unless reports are numerous, an interpolation scheme between station reports results in a poor estimate. A much more powerful approach was used by adapting a direct method of stream-function calculations from actual wind reports as proposed by Endlich and Mancuso (1964). This iterative procedure permits evaluation of the stream function at the stations. In a later report, Endlich and Mancuso (1965) included an objective analysis for the computation of the stream-function at grid points from those determined at the stations.

Charette (1971) applied the method of Endlich and Mancuso with only minor modifications to an area slightly larger than that indicated in Figure (2-2). However, some major changes were introduced into this scheme in the present study.

The surface-wind field was derived from a scalar objective analysis using a correction method which bears some similarity to that proposed by Cressman (1959). This essentially amounts to an elaborate interpolation scheme but, at the earth's surface, it was felt that reports were sufficiently abundant to allow this. It was found that with a

minimum of modification this same procedure could be applied to the temperature and dewpoint fields at ground level. The scalar objective analysis is also used at upper levels to estimate the temperature and dewpoint at grid points with the realization that the derived fields may be in error in data sparse regions.

3.2 The Stream-Function: A Brief Review

Consider flow parallel to the x-y plane for an incompressible fluid. It can then be shown (see e.g. Whitaker (1968)) that the mass flow rate across an arbitrary curve between two points is independent of the path chosen. That is $\vec{V}\cdot\hat{n}$ ds is an exact differential of some function ψ, where $\vec{V}$ is the velocity vector along the curve, $\hat{n}$ is a unit vector normal to the curve, and ds, an elemental distance along the curve. This function is known as the stream-function, and the differential $d\psi$ expressed as a function of x-y coordinates is:

$$d\psi = (\frac{\partial \psi}{\partial x})dx + (\frac{\partial \psi}{\partial y})dy ; \qquad (3-1)$$

but

$$d\psi = \vec{V}\cdot\hat{n} \; ds = u \; n_x \; ds + v \; n_y \; ds \qquad (3-2)$$

where u, v and n_x, n_y are the components of $\vec{V}$ and $\hat{n}$. Let $\vec{t}$ be a unit vector tangent to the curve joining the points mentioned above. It is easily shown that:

$$0 = \hat{n}\cdot\hat{t} = n_x\frac{dx}{ds} + n_y\frac{dy}{ds} \qquad (3-3)$$

and therefore

$$n_x = \frac{dy}{ds} \text{ and } n_y = \frac{dx}{ds} \qquad (3-4)$$

The signs in expression (3-4) could be reversed and still satisfy equation (3-3), but the signs in (3-4) are retained in the subsequent steps. By equating equations (3-1) and (3-2) and substituting for n_x and n_y from (3-4),

$$(\frac{\partial\psi}{\partial x} - v)dx + (\frac{\partial\psi}{\partial y} + u)dy = 0 \ . \tag{3-5}$$

As equation (3-5) applies for any curve with the implication that dx and dy are not identically zero in every case, it follows that:

$$u = -\frac{\partial\psi}{\partial y} \quad \text{and} \quad v = \frac{\partial\psi}{\partial x} \ . \tag{3-6}$$

Hess (1959) defines a streamline in the following manner:

A streamline is a line to which, at any given instant, are tangent all the velocity vectors of the points through which the line passes; thus the flow is along the streamlines at any given moment.

Along a streamline the velocity vector is $|\vec{V}|\ \hat{t}$ and the difference in the stream-function at two points A and B:

$$\psi_B - \psi_A = \int_A^B d\psi = \int_A^B |\vec{V}|\ \hat{t}.\hat{n}\ ds = 0 \tag{3-7}$$

Thus, at a given instant, a line joining points of a constant stream-function is a streamline.

In the atmosphere, flow may be treated as incompressible if the divergence is zero or vanishingly small. Like vertical velocity, divergence in the atmosphere cannot be measured directly because of its small magnitude and the errors in wind measurements from pilot balloon or radiosonde ascents. The next section is based on the assumption that the divergence is zero so that the two dimensional flow is completely

described by the stream-function which accounts for vorticity, translation and deformation. Application of this assumption to mountainous regions may result in a grossly simplified picture of the true flow, but it is believed that such a treatment is considerably better than the assumption of a geostrophic balance.

3.3 Stream-Function Calculation at Stations

Substitution of equation (3-6) into (3-1) yields the stream-function differential $d\psi$ between two nearby points:

$$d\psi = v \, dx - u \, dy \qquad (3-8)$$

or, in finite difference form,

$$\Delta\psi = v\Delta x - u\Delta y \quad . \qquad (3-9)$$

The stream-function has dimensions (L^2/T). It is convenient to define a modified stream function:

$$\overset{*}{\psi} = \frac{f}{9.8} \psi \qquad (3-10)$$

where f = Coriolis parameter. The modified stream-function now has the same dimensions (L^2/T^2) as geopotential height. This manipulation allows comparison with the original height field which is also expressed in geopotential units. Therefore equation (3-9) becomes:

$$\Delta\overset{*}{\psi} = \frac{f}{9.8} (v\Delta x - u\Delta y) \qquad (3-10a)$$

The difference in the modified stream-function between a station o and a nearby station i is:

$$\Delta\overset{*}{\psi}_i = \overset{*}{\psi}_o - \overset{*}{\psi}_i \quad .$$

Thus, the modified stream-function at the station o may be estimated from:

$$\overset{*}{\psi}_o = \overset{*}{\psi}_i + \Delta\overset{*}{\psi}_i$$

In their earlier paper, Endlich and Mancuso (1964) evaluated $\Delta\overset{*}{\psi}_i$ from the expression:

$$\Delta\overset{*}{\psi}_i = \frac{f_0 + f_i}{9.8}\left[\frac{(v_0 + v_i)(x_0 - x_i) - (u_0 + u_i)(y_0 - y_i)}{4}\right]$$

(3-11)

where g has been replaced by 9.8 in agreement with equation (3-10). In the free atmosphere, flow is very closely geostrophic and is given by the vector product:

$$\vec{V} = \frac{9.8}{f}\hat{k} \times \nabla Z ,$$

(3-12)

where Z is the height of a constant pressure surface in geopotential meters (gpm) and $\hat{k}$ is a unit vector normal to the horizontal plane. The stream-function also determines the wind from:

$$\vec{V} = \hat{k} \times \nabla\psi = \frac{9.8}{f}\hat{k} \times \nabla\overset{*}{\psi}$$

(3-13)

In middle latitudes, the geostrophic balance is a good approximation to the actual wind field so that:

$$\nabla\overset{*}{\psi} = \nabla Z .$$

(3-14)

In their 1965 version of the stream-function computation, Endlich and Mancuso used a weighted combination of winds and heights given in equation (3-15):

$$\Delta\overset{*}{\psi}_i = \frac{f_0 + f_i}{2 \times 9.8} w_1 \left[(v_0 + v_i)(x_0 - x_i)\right.$$
$$\left. - (u_0 + u_i)(y_0 - y_i)\right] + w_3(Z_0 - Z_i)$$

(3-15)

where w_1 and w_3 are weights with empirically determined values of 0.45 and 0.10 respectively.

Extensive testing of both equations (3-11) and (3-15) revealed rather large discrepencies between the input height field and the final field of the modified stream-function. Changes as large as 60 gpm were observed on occasion, and, more frequently adjustments greater than 30 gpm. Convergence within a prescribed limit of 0.5 gpm was much faster using equation (3-15), but some major differences appeared between the two modified stream-function fields when the same data were used for input.

Despite the disadvantage of requiring more computer time, equation (3-11) was used in the final model, as the assumption that the flow was geostrophic in mountainous regions, needed to justify equation (3-15), was apparently violated. Charette used equation (3-15) in his model.

More than one estimate of $\overset{*}{\psi}_0$ is possible when the number of neighbouring stations is high. If there are n such estimates, then an averaged estimate might be:

$$\overset{*}{\psi}_0 = \frac{1}{n} \sum_{i=1}^{n} (\psi_i + \Delta\overset{*}{\psi}_i) \qquad (3-16)$$

A procedure suggested by Endlich and Mancuso (and followed by Charette) was to compute two such averages. One average $(\overset{*}{\psi}_0)_1$ is obtained from all the stations within 300 miles of the station o, and a second averaged estimate $(\overset{*}{\psi}_0)_2$ from stations located between 300 and 550 miles from station o. These two estimates are combined as:

$$\overset{*}{\psi}_0 = A_1(\overset{*}{\psi}_0)_1 + A_2(\overset{*}{\psi}_0)_2 \, , \qquad (3-17)$$

where A_1 and A_2 are weighting factors assigned values 0.8 and 0.2, justified by the statement that:

> the observations are weighted more or less
> inversely with distance from the point of
> interest ...
> (Endlich and Mancuso, 1964)

A search for a better weighting scheme was undertaken, since the one given above is not only awkward to program, but is also discontinuous and arbitrary. An alternative which was tested is simply:

$$A = 1 - (r/R)^2 = \frac{R^2 - r^2}{R^2} \quad \text{for } r \leqslant R$$

$$A = 0 \qquad\qquad\qquad \text{for } r > R \tag{3-18}$$

where R = a set radius of influence

  r = separation between two stations.

It was found that although a generally smooth pattern was attained, in those areas where there was greater station density, the calculated stream-function was not particularly sensitive to an individual report. The wind field from such an analysis did not agree well with a particular wind report but was an average of the winds at surrounding stations. Cressman used:

$$A = \frac{1 - (r/R)^2}{1 + (r/R)^2} = \frac{R^2 - r^2}{R^2 + r^2} \quad \text{for } r \leqslant R \tag{3-19}$$

which gives slightly less weight to the stations in the range 0<r<R (see Figure 3-1) than equation (3-18). A linear decrease with distance is given by:

$$A = 1 - (r/R) = \frac{R-r}{R} \quad \text{for } r \leqslant R \tag{3-20}$$
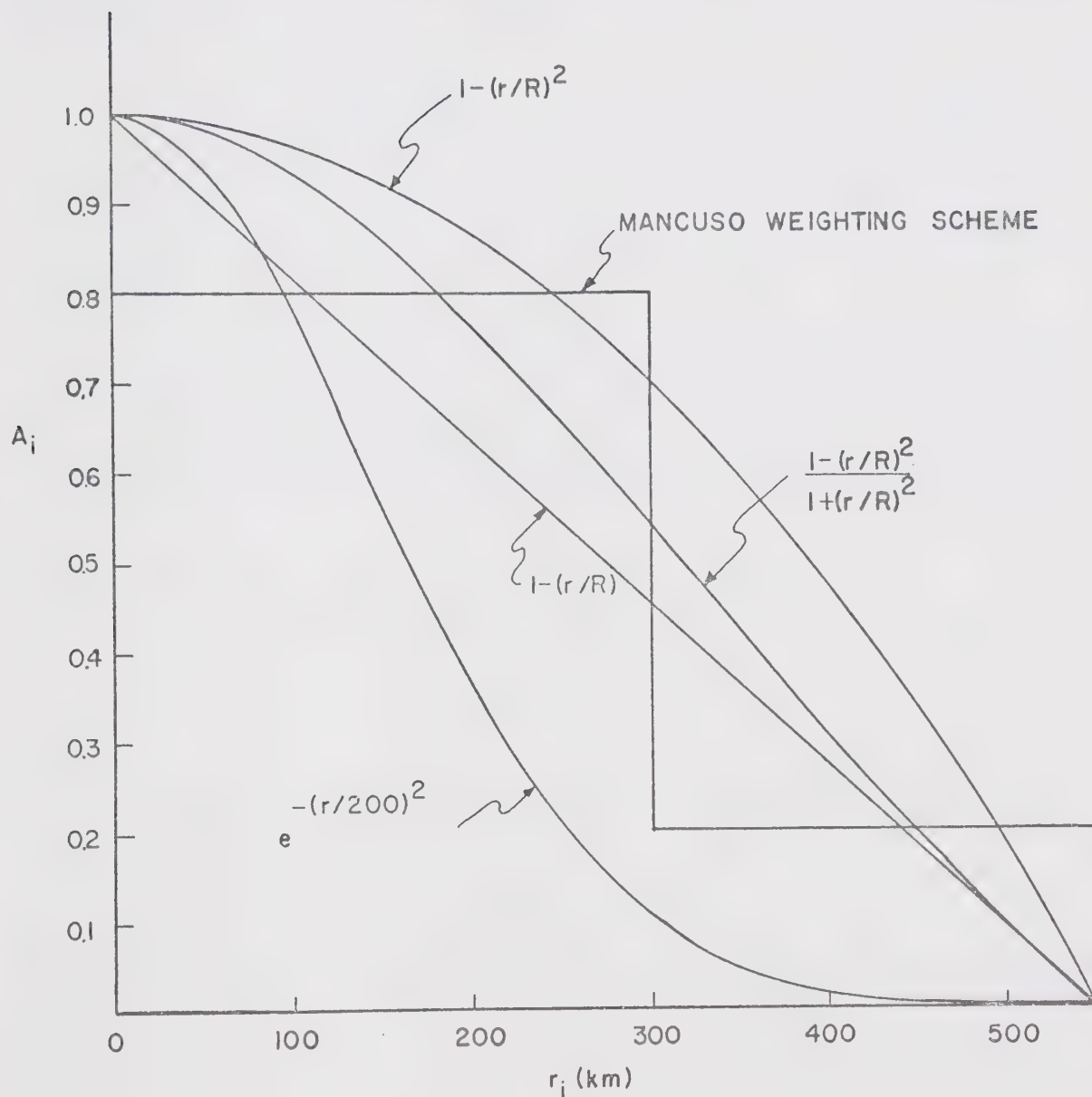
FIGURE (3-1) A comparison of various weighting functions dependent upon distance of separation.

Neither of the last two weighting functions was considered significantly
different from expression (3-18). A weighting factor which is close
to unity when the station separation is small and decreases to near
zero much more rapidly than any of above with increasing station separa-
tion is:

$$A = \exp\text{-}(r/c)^2 \qquad\qquad (3\text{-}21)$$

where c is a constant which may be set to any value greater than zero.
In this study the value of c was set equal to 200 and r was expressed in
kilometers.

Equation (3-21) determines the relative weights of the estim-
ates of the stream-function at a particular station from its neighbours
with a radius of influence of 600 kilometers. A weighted mean is given
by:

$$\overset{*}{\psi}_0 = \frac{\sum\limits_{i=1}^{n} A_i(\overset{*}{\psi}_i + \Delta\overset{*}{\psi}_i)}{\sum\limits_{i=1}^{n} A_i} \qquad . \qquad\qquad (3\text{-}22)$$

Reports of wind speed and direction, and geopotential height
were extracted from plotted and analyzed synoptic charts at 850 mb,
700 mb and 500 mb. Pilot balloon reports did not have the heights of
the pressure surface at their locations so that bogus data were inserted
for the heights. In the first scan, these abnormal values were recog-
nized and not used as initial guesses of the modified stream-function.
Heights from radiosonde reports were used to establish the estimate of
the modified stream-function at a pilot balloon station by the stream-
function calculation. The new estimate of $\overset{*}{\psi}_0$ was immediately substi-

tuted for the former estimate in much the same manner as a sequential
relaxation. This had two main advantages over updating the field simul-
taneously after a scan of all stations was completed:

    (a) convergence of $\overset{*}{\psi}$ at all stations to within .5 gpm

           was much faster.

    (b) computer storage requirements were reduced.

On any particular scan a record is kept of the maximum
alteration between the present and previous estimates of $\overset{*}{\psi}$. If this
maximum value is greater than .5 gpm another complete pass of all
stations is made. As soon as the maximum alteration drops below this
limit, the computation is terminated. In no instance did the field fail
to converge, although it was noted that the magnitude of the alterations
decreased very slowly from 1 gpm to .5 gpm, particularly with a large
number of stations. Convergence to within 1 gpm usually took from 6 to
8 iterations independent of the number of stations. It is possible
that machine truncation error was responsible for the effects mentioned
above. From experience, it is now felt that 1 gpm would be a more
practical limit.

Another feature of interest was that a slightly faster conv-
ergence resulted when the stations were ordered in such a way that the
computations began with stations along the outer edge of the map and
"spiralled" in toward the centre in the initial testing. Data were there-
fore ordered in this fashion in all the cases investigated in Chapter 5.

No adjustment was made to the final field as was done by
Charette or Endlich and Mancuso, because the station density was not

uniform in all regions. Charette's adjustment method is open to objection on the grounds that it also changes the gradient of the $\overset{*}{\psi}$ over the entire map.

3.4 Objective Analysis of Modified Stream-Function

Once the values of $\overset{*}{\psi}$ are known at the stations it is necessary to estimate $\overset{*}{\psi}$ at the nearby grid points. Let ℓ be a grid point near station i. Then $\overset{*}{\psi}$ at ℓ may be calculated to be:

$$\overset{*}{\psi}_{\ell} = \overset{*}{\psi}_i + \Delta\overset{*}{\psi}_i \tag{3-23}$$

where

$$\Delta\overset{*}{\psi}_i = \frac{f_{\ell} + f_i}{9.8}\left[\frac{v_i(x_{\ell} - x_i) - u_i(y_{\ell} - y_i)}{2}\right] \tag{3-24}$$

If there are n such stations then:

$$\overset{*}{\psi}_{\ell} = \frac{\displaystyle\sum_{i=1}^{n} A_i(\overset{*}{\psi}_i + \Delta\overset{*}{\psi}_i)}{\displaystyle\sum_{i=1}^{n} A_i} \tag{3-25}$$

where A_i is a distance-dependent weighting factor as given in equation (3-21). Again this differs from the weighting scheme used by Endlich and Mancuso (1965), but it is considerably easier to implement and not discontinuous.

At the sacrifice of using increased storage, the calculations are performed from the point of view of a given observing station. From the station's latitude and longitude it is possible to determine the station location in grid coordinates. A radius of influence of 600 km is used. Many of the stations used in the $\overset{*}{\psi}$ calculation lie outside the grid and may only influence a few of the outer rows or columns. The

range of indices of the rows and columns which include all the grid
points within 600 kilometers of the station can be computed. Points near
the corners of this region are not within the 600 km criterion, but as r
is calculated for the weighting function anyway, these points are easily
excluded. A weighted estimate and a weight are computed for each grid
point within 600 km. Then the next station is considered. Each new
weighted estimate is added to the sum of previous estimates at the grid
point, as are the weights. This requires two matrices equal to the size
of the grid. Once the stations are exhausted, the weighted mean is
calculated at each grid point from equation (3-25).

The modified stream-function may be used to evaluate the u and
v components of the wind with respect to the grid from:

$$u_\psi = - \frac{9.8}{f} \frac{\partial \overset{*}{\psi}}{\partial y} \qquad (3\text{-}26a)$$

$$v_\psi = + \frac{9.8}{f} \frac{\partial \overset{*}{\psi}}{\partial x} \qquad (3\text{-}26b)$$

If one replaces H by $\overset{*}{\psi}$ in Figure (2-8) the following finite difference
approximations may be used to evaluate the wind components at the centre
of each grid square:

$$u_\psi = - \frac{9.8 \, \sigma}{2 \, df} \left(\overset{*}{\psi}(I,J) + \overset{*}{\psi}(I,J+1) - \overset{*}{\psi}(I+1,J) - \overset{*}{\psi}(I+1, J+1) \right)$$

$$(3\text{-}27)$$

and

$$v_\psi = \frac{9.8 \, \sigma}{2 \, df} \left(\overset{*}{\psi}(I,J) + \overset{*}{\psi}(I+1,J) - \overset{*}{\psi}(I, J+1) - \overset{*}{\psi}(I+1, J+1) \right)$$

$$(3\text{-}28)$$

where σ = image scale

   d = grid length at 60°N

   f = coriolis parameter

$\overset{*}{\psi}$ is also used as an estimate of the height of the constant pressure

surface. If the mean value of $\overset{*}{\psi}$ at the centre of the grid square as determined by an average of $\overset{*}{\psi}$ at the corners is less than H, then u and v are set equal to zero since the pressure surface would be below the terrain and no flow exists.

3.5 The Scalar Objective Analysis

A means was sought to estimate the wind field at the surface. The assumptions of a geostrophic balance are not valid because of the proximity of the surface which exerts a frictional force on an air parcel. Divergence at this level is large so that the stream-function cannot be used to represent the total wind field. As a rough approximation the wind at the stations was expressed in component form with respect to the grid. If S is the wind speed and D is the direction of the wind in degrees measured clockwise from true north, then the components are:

$$u = S \cos(350 - D - \lambda)$$
$$v = S \sin(350 - D - \lambda)$$

(3-29)

where λ = longitude of the station.[1]

On the first scan, a radius of influence of 700 km is used. The method of applying the estimates of u and v at the grid points is identical to that given in the previous section with the exception that equation (3-30) lacks a term analogous to $\Delta\overset{*}{\psi}$. Let X be any variable for which a value is known at the station. Then:

$$X_\ell = \frac{\sum_{i=1}^{n} A_i X_i}{\sum_{i=1}^{n} A_i}$$

(3-30)

[1]See Appendix A for details of derivation.

where A_i = weighting factor as before. As may be expected, the first pass yields a very smoothed representation. Therefore, three more scans are made reducing the radius of influence by 200 km each time. On each scan after the first a correction term C_ℓ is computed from:

$$C_\ell = \frac{\sum\limits_{i=1}^{n} A_i (X_i - X_\ell^o)}{\sum\limits_{i=1}^{n} A_i} \qquad (3\text{-}31)$$

and
$$X_\ell' = X_\ell^o + C_\ell \qquad (3\text{-}32)$$

If only one station influences a grid point then:

$$C_\ell = A_i (X_i - X_\ell^o) \qquad (3\text{-}33)$$

The final scan has a radius of influence of 100 km which is sufficient to give reasonable resolution. It might be practical to change the value of c in equation (3-21) but such a refinement was not investigated.

Originally this method was designed to derive an initial guess field for a scalar objective analysis developed by the Navy Fleet Numerical Weather Central described in Haltiner (1971) but the FNWC analysis made only slight alterations to the field of χ computed by the procedure above. It was felt that these alterations were not of sufficient importance to justify the additional program complexity and computer running time.

If data were missing the station was rejected from consideration. This scheme, with slight input-output modifications, was found readily adaptable to derivation of temperature and dewpoint fields at all levels, although its ability at upper levels is hampered because data density is substantially reduced.

CHAPTER 4

OROGRAPHIC PRECIPITATION COMPUTATION

4.1 Introduction

The vertical velocities as calculated in this model may be a
crude approximation of the real state of the atmosphere or at times even
totally erroneous. Without doubt many important processes have been
overlooked. For example, a study by Hess and Wagner (1948) of isentropes
over the mountainous region of the northwestern United States clearly
indicates that motion is much more complex than that depicted here. How-
ever, there is at least one way of assessing the ascending motions
computed, and that is through the realization of precipitation. It is
not sufficient to evaluate simply the occurrence or non-occurrence of
precipitation, but the recorded amounts of precipitation should bear some
resemblance to the vertical motions responsible for the rain's formation.

Attempts to calculate precipitation quantitatively have been
made by Smagorinsky and Collins (1955) and by O'Neill (1966) based on
computed vertical velocity fields. Both use a very simplified rain
model which dates back to a paper by Fulks (1935). A similar approach
is used here.

4.2 Rate of Precipitation

One of the most vital areas of meteorology and at the same time
one of the most elusive is cloud physics. Ascending vertical motion is

a necessary but not sufficient condition for the formation of rain. Important refinements to the theory of the growth of a single isolated rain drop have been made by Fukuta and Walter (1970), but as yet a totally satisfactory explanation and model of the growth of rain droplets in a cloud is lacking. In view of this and other difficulties a simple approach is taken.

To utilize Fulks expression for the rate of precipitation a number of drastic assumptions are required:

(a) condensation nuclei are sufficiently numerous so that condensation commences the moment the saturation temperature is achieved.

(b) on the scale of motion considered, temperature changes for an air parcel occur adiabatically.

(c) water storage within a cloud is ignored.

(d) no evaporation of precipitation takes place between the cloud and the ground.

The above is a summary of a discussion found in Pettersen (1956b, Vol. 2). In a more concise fashion, it is assumed that any condensation is the result of pseudo-adiabatic cooling, and condensation which occurs at the saturation temperature results in precipitation at the ground.

Consider a volume of air of unit cross-section and height ΔZ. The total water vapour in the volume is $\rho q \Delta Z$ where ρ is the density of dry air and q is the mixing ratio. The rate of precipitation must equal the rate of condensation from the assumptions stated. Let

$$P_i \; = \; - \rho \frac{dq}{dt} \Delta Z \qquad\qquad (4\text{-}1)$$

be the rate of precipitation and note that dq/dt is the condensation which results from removal of moisture from the volume (and hence the negative sign). The vertical velocity may be expressed as $w = dZ/dt$ and if it is possible to neglect changes in the thickness ΔZ then:

$$P_i \;=\; -\rho \frac{dq}{dZ}\, w\, \Delta Z \tag{4-2}$$

but

$$q \;=\; \frac{0.622e}{p-e}$$

and

$$\frac{dq}{dZ} \;=\; \frac{0.622}{(p-e)^2}\left[(p-e)\frac{de}{dZ} - e\,\frac{d(p-e)}{dZ}\right] \tag{4-3}$$

where e = saturation vapour pressure. The vapour pressure e is usually very small in comparison to the total atmospheric pressure at any level so that:

$$\frac{dp}{dZ} \;=\; -\,g\rho \;\simeq\; -\,\frac{pg}{R_d T} \tag{4-4}$$

where R_d = gas constant for dry air,

and $\quad$ T = the absolute temperature,

and $\quad \rho$ = density of the air.

Equation (4-3) may be simplified by expanding the terms in the square brackets and substituting for dp/dZ from (4-4).

$$\frac{dq}{dZ} \;=\; \frac{0.622}{\rho\, R_d T}\left(\frac{de}{dZ} + \frac{e\,g}{R_d T}\right)$$

This in turn may be substituted into equation (4-2). Then:

$$P_i \;=\; -\,\frac{0.622}{R_d T}\left(\frac{de}{dZ} + \frac{eg}{R_d T}\right) w\Delta Z \tag{4-5}$$

At saturation, all the water vapour terms can be calculated so that a knowledge of w yields the precipitation rate.

The expression de/dZ can be evaluated by the use of the chain rule, i.e.

$$\frac{de}{dZ} = \frac{de}{dT}\frac{dT}{dZ} \qquad (4-6)$$

It is assumed that condensation occurs at temperatures below the freezing point of water, and thus for all temperatures in the normal meteorological range:

$$e = 6.11 \exp\left[\frac{m_v L_v}{R^*}\left(\frac{1}{273} - \frac{1}{T}\right)\right] \qquad (4-7)$$

from the Clausius-Clapeyron equation and:

$$\frac{de}{dT} = \frac{m_v L_v}{R^* T^2} e$$

where R^* = universal gas constant

L_v = latent heat of evaporation of water at 273° Kelvin.

To determine dT/dZ, Fulks used an equation derived by Brunt (1933) for the pseudo-adiabatic lapse rate, but a simpler expression is given by Hess (1959):

$$\frac{dT}{dZ} = -\frac{g}{c_p}\left[\frac{1 + \left(\frac{L_v}{R_d}\frac{q}{T}\right)}{1 + \left(\frac{L_v q}{R_d T}\right)\left(\frac{0.622 L_v}{c_p T}\right)}\right] \qquad (4-8)$$

where c_p = heat capacity at constant pressure for dry air.

This ignores the heat capacity of the liquid water and the change of the latent heat of evaporation with temperature. If the atmosphere is div-

ided into a number of layers, then the total precipitation at the ground from a column of unit cross-section is:

$$P = \sum_{i=1}^{n} P_i \qquad (4\text{-}9)$$

There are two ways of viewing the situation. If equation (4-5) is considered from the point of view of a parcel of thickness ΔZ, the rate of precipitation due to that volume will decrease as the temperature decreases, even though w may remain constant. Eventually, at some very low temperature, virtually all the moisture will have condensed and the precipitation rate will be reduced to zero. However, if the parcel just considered is replaced by another saturated parcel with initial conditions equal to the previous one, then over a particular position the rate of precipitation for layer i remains the same. The second case is far more instructive, and multiplication by a time period Δt results in the precipitation which should be realized at that position over the time interval.

O'Neill assumed that saturated conditions were present whenever ascending motions were calculated, in order to simplify his precipitation calculations, but this is not necessary. Let the total ascent over a time interval Δt be:

$$Z = w \Delta t \qquad (4\text{-}9)$$

If the parcel is initially unsaturated then part of the ascent (Z_1) is required to reach saturation. Thus only $\Delta t'$ of the total time increment Δt is really amenable to the treatment of Fulks. An effective vertical velocity w' may be determined by:

$$Z = Z_1 + Z_2$$
$$= Z_1 + w \Delta t'$$

but $\qquad$ $w' \Delta t = w \Delta t'$

and $\qquad$ $Z = Z_1 + w' \Delta t$ $\qquad$ (4-10)

The lift required for saturation is:

$$Z_1 = \frac{T_0 - T_{do}}{\gamma d - \gamma dd} \qquad (4-11)$$

where $\quad T_0$ = initial temperature of parcel

$\qquad T_{do}$ = initial dewpoint temperature of parcel

$\qquad \gamma_d$ = lapse rate of temperature

$\qquad \gamma_{dd}$ = lapse rate of dewpoint temperature

It can be shown that to a close approximation (see e.g. Pettersen (1956b Vol. 2):

$$\gamma_d - \gamma_{dd} \doteq 0.83^o\text{K per 100 meters.}$$

Therefore

$$w' = w - \frac{T_0 - T_{do}}{0.83 \Delta t} \qquad (4-12)$$

4.3 The Rain Model

Equation (4-12) was used to calculate an effective vertical velocity over the time period Δt. The parameters of temperature, dewpoint temperature, vertical velocity and heights of surfaces for which the previous fields were known for the entire grid were entered.

The normal case of the 850-mb surface situated above ground level was dealt with in a straight forward manner. The layer between the surface and 850 mb was divided into two sub-layers. The lower half was assigned the vertical velocity computed for the surface. The temperature and dewpoint at the middle of the first sub-layer were computed from the gradients from the surface to 850 mb. The next layer was the

upper half of the one just considered plus the lower half of the 850
to 700-mb layer. The last layer includes the upper half of the 850 to
700-mb layer the lower half of that from 700 to 500 mb. The attributes
of the 850 and 700 mb levels were assigned to the last two layers,
respectively.

If the vertical velocity in a layer was negative or zero, the
precipitation for that layer was set to zero. Next, the layers with
positive vertical velocities of greater than 10 cm/sec were rejected and
the precipitation set to an arbitrarily high value. Vertical motion in
excess of 10 cm/sec was thought to exceed the assumption that precipi-
tation is immediately realized at the ground. Sawyer (1956) and others
recognize that such is not the case, and that a considerable time lag
exists between the initial condensation and growth to rain drop size.
Heavy precipitation is likely to be associated with these sizable ascent
rates, but a more sophisticated approach is required to evaluate it.

If $0 < w < 10$ cm/sec, then the ascent required for saturation
was determined from equation (4-11). The saturation temperature was
calculated at this level, and the effective ascent rate w' for a 6 hour
period determined. If w' was less than zero, saturation was not achieved
and the layer's precipitation set to zero. If all the above conditions
were avoided, the precipitation rate was calculated using equation (4-5)
and multiplied by Δt equal to 6 hours. By summing the contribution
of the layers, the rain for a given grid position was determined. The
amount first calculated in centimeters was converted to inches for com-
parison with surface reports of precipitation.

When the surface was above the 850-mb level, the computed
surface vertical velocity was retained, but the temperature and dewpoint

were replaced by a linear interpolation between 850 and 700 mb. The calculations then proceeded as outlined above.

The vertical velocity at 500 mb was set equal to zero as the orographic vertical velocity at that level was zero everywhere, except in a test case where a positive value of 1 cm/sec was observed.

Obviously this model requires considerable refinement but as a first approximation it performed reasonably well. The results are presented in Chapter 5.

CHAPTER 5

RESULTS

5.1 Introduction

Three synoptic situations are presented in this chapter. In
each case an analyzed stream-function map is given for the 850-mb,
700-mb and 500-mb levels. The computed vertical velocities are analyzed
on separate charts at the 850-mb and 700-mb levels because the patterns
derived at one-eighth grid length with the original terrain are much
more complex than those found by Charette (1971). Orographic vertical
velocities at 500 mb are in all cases zero but the 500-mb stream-
function analysis is shown to illustrate the performance of the ψ^* cal-
culation when data are scarce. In addition, the orographic vertical
velocities associated with surface winds are illustrated in each case.
Isotachs of vertical velocity are drawn at 5, 10 and 40 cm/sec while ψ^*
is analyzed at 30-gpm increments.

Included with the first example is a subjective analysis of
the 850-mb constant pressure map for comparison with the ψ^* chart
computed for the same level.

The rain model was applied to the second case only. In this
instance, maps of computed orographic rain, actual reported rain, and
the objective temperature analysis at the surface are shown in addition
to those mentioned above.

5.2 October 14, 1960 - 00Z[1]

5.2.1 The Synoptic Situation

A deep low is centred 500 kilometers south of Kodiak Island, Alaska, while a weak ridge of high pressure dominates the circulation of Western Canada. In the course of the next 48 hours, the low tracks slowly northeast to the northern extremity of the Gulf of Alaska, providing a sustained westerly flow across the British Columbia coast. The associated frontal wave is observed to occlude out of the low and move eastward across British Columbia. Lee cyclogenesis over northeastern British Columbia is evident by 06Z on October 15.

5.2.2 Stream-Function Analyses

As mentioned earlier a subjective analysis (see Figure (5-1)) is given of the 850-mb pressure surface in this case only. It should be mentioned that it was analyzed with considerable care to maintain contour gradients consistent with wind reports as determined by a geostrophic wind scale. The original data were expressed in geopotential feet and the conversion is made from these units to gpm. Despite these precautions, the stream-function analysis (Figure (5-2)) was substantially different over the northeastern portion of the analyzed map. By drawing an intermediate contour, a closed high circulation is noted over the central Yukon which is not suggested by the subjective height analysis. In addition, the $\overset{*}{\psi}$ analysis indicates a sharp trough in northwestern Alberta of which there is no indication on the subjective

---

[1]refers to Greenwich Mean Time

analysis. The strong gradient along the left edge of the $\overset{*}{\psi}$ analysis
is thought to be due to the lack of reports in that area.

Of all the objective $\overset{*}{\psi}$ analyses, the one of the 700-mb wind-
field (Figure (5-3)) is probably the poorest. In this case, it is felt
that the iterative procedure has been pushed beyond its capability.
The $\overset{*}{\psi}$ gradient over northern British Columbia appears excessive and is
believed due to the lack of reports in that area. As well, it can be
seen that Annette and Fort Nelson are too widely separated for either
to influence the other in the iterative procedure, and similarly
Whitehorse and Prince George. Where the flow is uniform this may not
be too critical, but the presence of both a trough and a ridge in close
proximity in this data sparse region would necessitate more information
for better resolution. Over the southern region of the map where data
are more abundant no peculiarities appear. In fact it is of interest
to note a diffluence of the streamlines in the vicinity of the Alberta
Range of the Rocky Mountains. Also of interest is the presence of a
trough over northeastern British Columbia, substantiating the feature
at 850 mb.

At the 500-mb level, the radius of influence was expanded to
700 km. The results shown in Figure (5-4) are encouraging. The main
problem area in the top left corner of the map is attributed to same
problem as above. Again, troughing is present over north-central
British Columbia. On the charts from which the wind data were extracted,
the analyst failed to notice this feature at any of the levels analyzed.
The trough provides the upper-air support for a minor wave on the arctic
front which travelled rapidly eastward across northern Saskatchewan and
Manitoba in the 12 hours following these maps.

On the next series of maps at 12Z it will be seen that the trough has also propagated rapidly eastward and is no longer within the analyzed area. The recognition of such minor features by the stream-function analysis could prove to be operationally beneficial. In this case, it proved to be advantageous over a height-contour analysis at all three levels.

5.2.3 Vertical Velocity Fields

The terrain-induced vertical velocities at the surface (Figure (5-5)) illustrate a complex pattern of ascending and descending motions; however, some generalizations can be made. First, a large region of descent is observed along the eastern slopes of the Rocky Mountains south of $60^{o}N$. A parallel but narrower region of ascent lies along western slope. Vertical motions on the west coast reflect the irregular topography of that region. Associated with an offshore flow over the Alaska Panhandle are marked regions of descent, while to the south unorganized ascent appears over Vancouver Island, the western slopes of the Coastal Mountains and northwestern Oregon.

At the 850-mb level (Figure (5-6)) the flow pattern is better organized, showing a region of pronounced descent to the lee of Vancouver Island with strong ascent along its western edge, and on the windward slope of the Coastal Mountains. Also, the Alaska Panhandle is under the influence of stronger ascending motion in contrast to the surface.

At the 700-mb surface rapidly alternating areas of descent and ascent are evident (Figure (5-6)) over high terrain. The abnormally tight gradient over the Stikine Mountains mentioned previously makes this region one of the most active. Large areas of organized motion are not apparent.
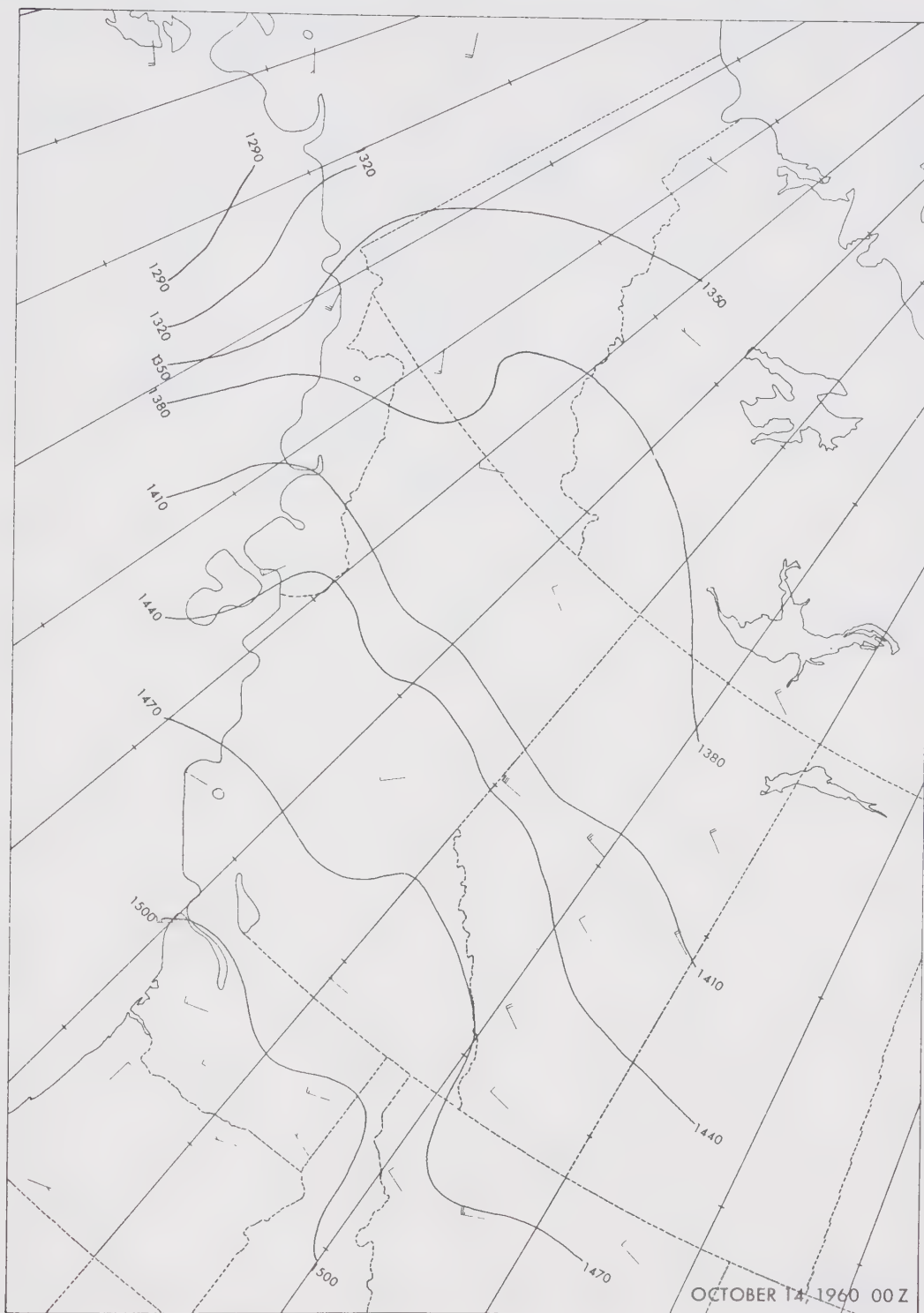
FIGURE (5-1) Subjective analysis of contour heights of the 850-mb pressure surface on October 14, 1960 - 00Z. Contours at 30-gpm intervals.
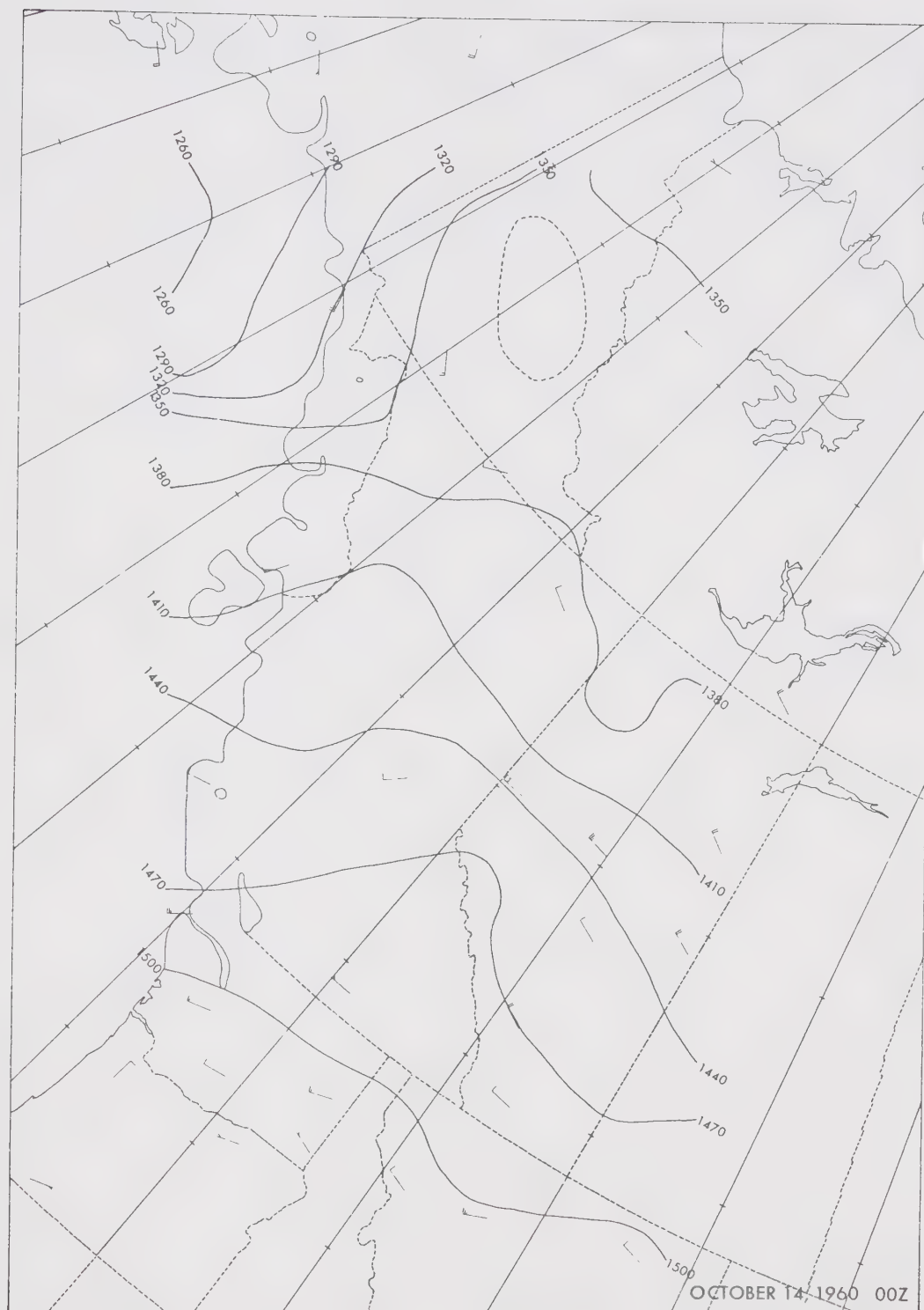
FIGURE (5-2) Modified stream-function analysis at 850-mb level on October 14, 1960 - 00Z. Contours drawn at 30-gpm intervals.
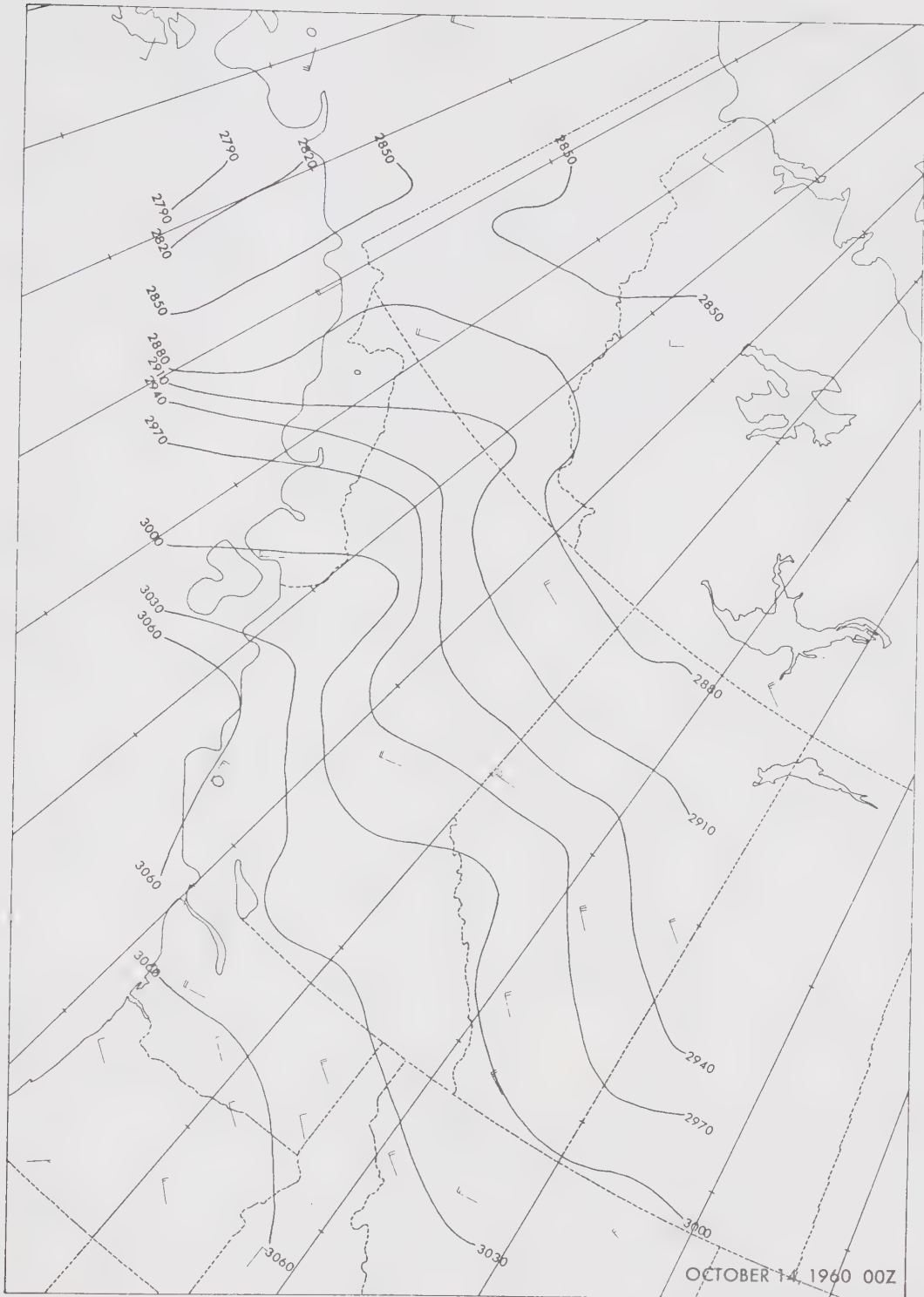
FIGURE (5-3) Modified stream-function analysis at the 700-mb level on October 14, 1960 - 00Z. Contours drawn at 30 gpm intervals.
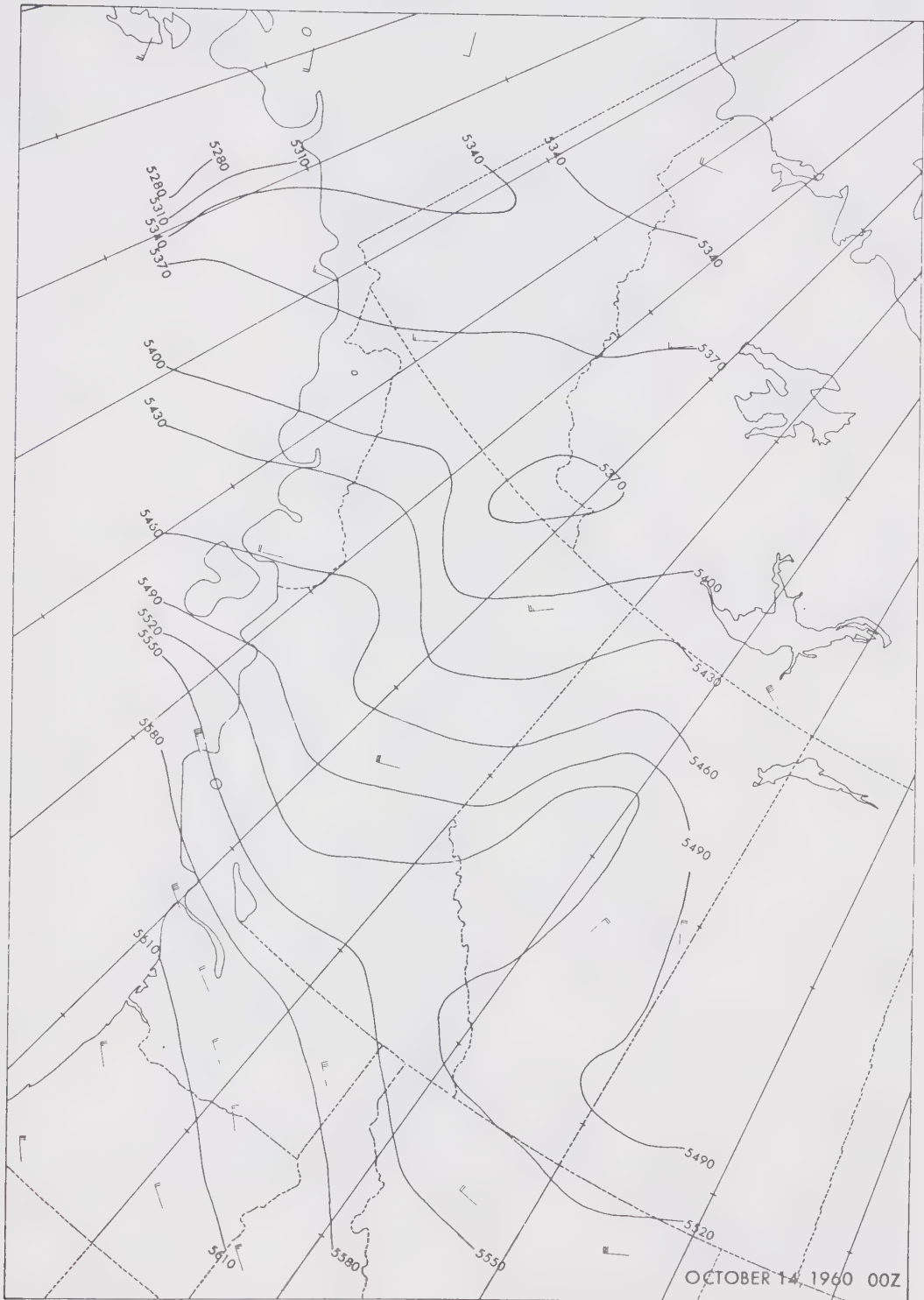
48

FIGURE (5-4) Modified stream-function analysis at the 500-mb level
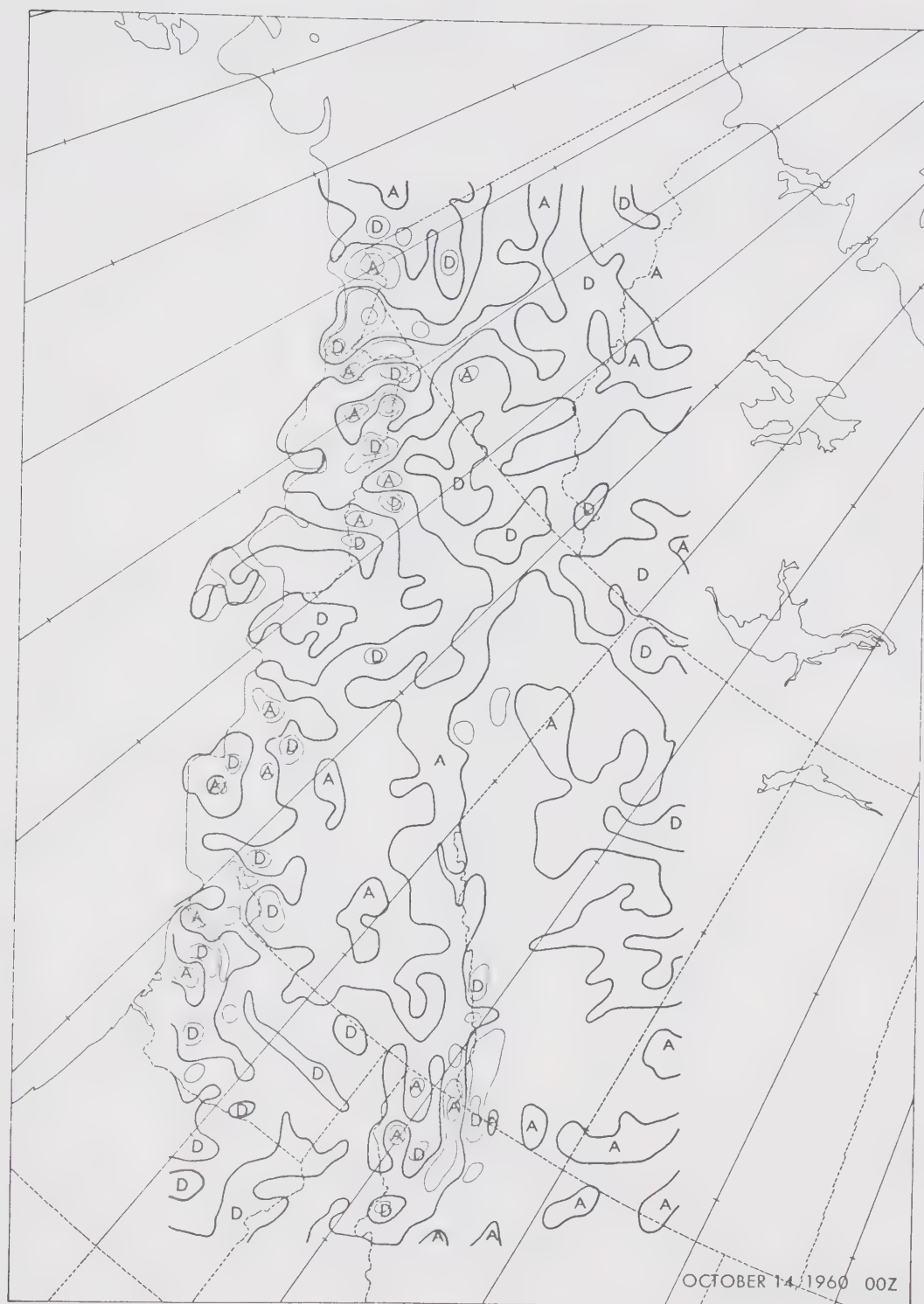on October 14, 1960 - 00Z. Contours drawn at 30-gpm intervals.

FIGURE (5-5) Surface vertical velocity induced by flow over sloping terrain on October 14, 1960 - 00Z. The heavy solid line separates regions of ascending and descending motion. Isotachs are drawn at 5, 10 and 40 cm/sec. The letters A and D represent ascent and descent respectively.
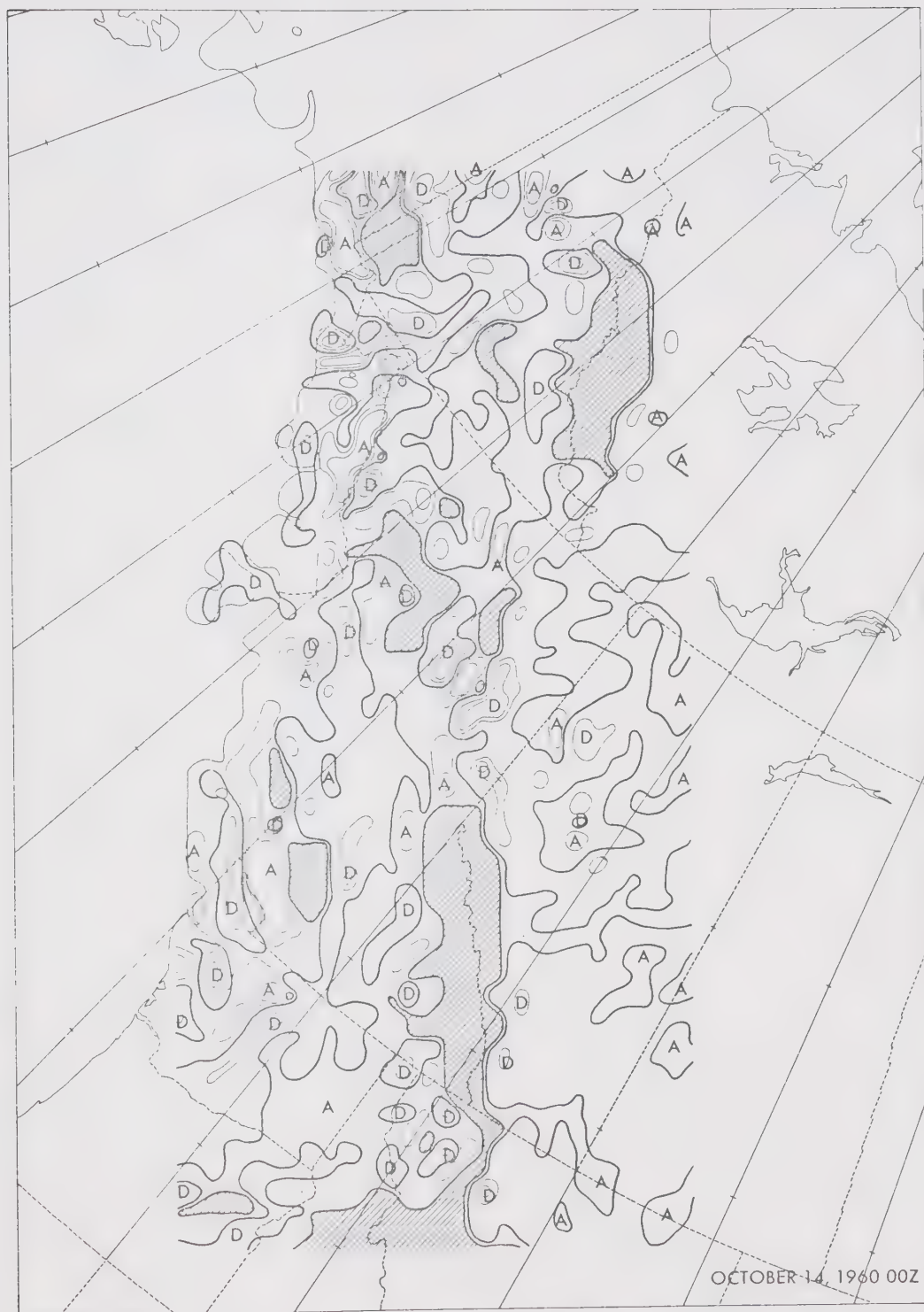
FIGURE (5-6) Terrain-induced vertical velocities at the 850-mb level
on October 14, 1960 - 00Z. Ascending and descending motions are marked
by the letters A and D respectively and are separated by a heavy solid
line. Isotachs at 5, 10 and 40 cm/sec. Shaded areas indicate surface
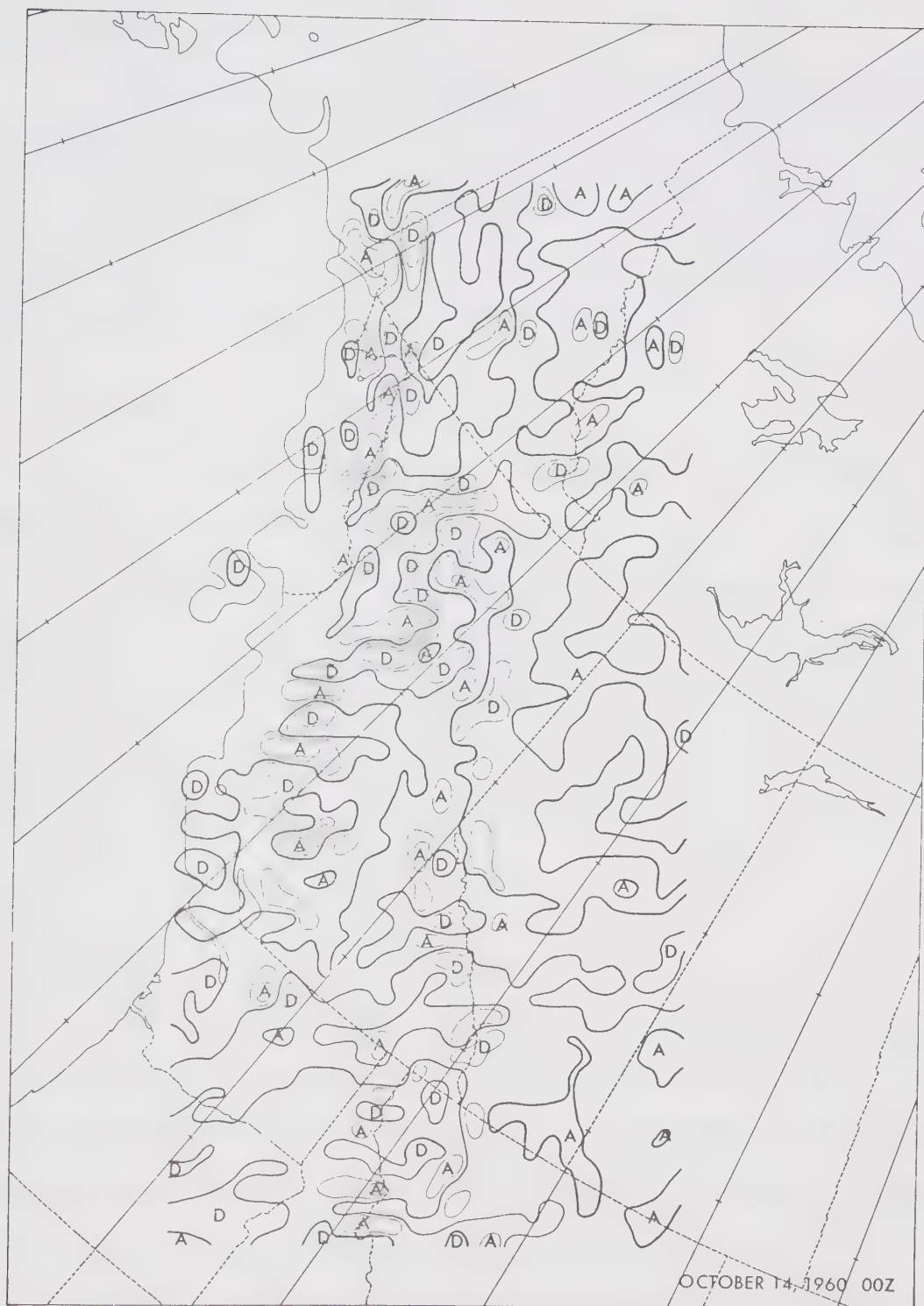below terrain.

FIGURE (5-7) Terrain-induced vertical velocities at the 700-mb level
on October 14, 1960 - 00Z. Ascent and descent are denoted by the
letters A and D respectively and separated by heavy solid line. Iso-
tachs at 5, 10 and 40 cm/sec.

5.3 October 14, 1960 - 12Z

5.3.1 Synoptic situation

This series of maps is just 12 hours later than those studied in the previous section. The low now occupies a position near the centre of the Gulf of Alaska and the associated frontal wave is analyzed to the northwest of the Queen Charlotte Islands. The circulation at the upper levels has increased markedly along the west coast.

5.3.2 Stream-Function Analyses

As a whole, the stream-function analyses in this series are handled much better than the earlier ones (see Figures (5-8), (5-9), (5-10)). The stronger winds ahead of the low are reflected by a tightening of the ψ^* gradient over the Alaska Panhandle. At the 850-mb a closed high is drawn just west of Jasper and a ridge over the same region is noted at the 700-mb level. This feature is not visible at the 500-mb level and is therefore presumed to be a reflection of flow around the major barrier of the Alberta Range.

5.3.3 Vertical Velocity Fields

At the surface (Figure (5-11)), many of the features noted 12 hours earlier are still present. The descending motion noted along the Alaska Panhandle is slightly more dominant as the offshore flow extends as far south as Vancouver Island. Slow descent covers much of Alberta except for marked descent near Pincher Creek (PC).

At the 850-mb level, the main change has been the increase in vertical motions associated with strengthening winds over the Alaska Panhandle. Also of interest are the vertical motions near the Swan Hills

in central Alberta, and over the Cypress Hills in southwestern
Saskatchewan (see Figure (5-12)).

Again, the 700-mb vertical velocity chart (Figure (5-10)) is
distinguished by its lack of organized motion, but to a lesser degree
than the 00Z case. Descent to the lee of Vancouver Island is well
marked, as is ascent along western slope of the Coastal Mountains in
southwestern British Columbia. Ascending motions of similar magnitude
to those shown on 00Z map along the western slope of the Rocky Mountains,
from west of Jasper northward, are still visible while descent prevails
to the lee of the same region.

5.3.4 Surface Temperature Objective Analysis

An illustration (see Figure (5-14)) of the derived temperature
field at the surface using the scalar objective analysis discussed in
Chapter 3 is included here. A total of 78 stations are used as input so
that reasonable detail is possible. The dewpoint temperature analysis
is not shown, but the pattern is similar. Since the temperatures at the
surface are normally reported in degrees Fahrenheit, the values given on
the analyzed map are also in Fahrenheit. However, temperatures are con-
verted to degrees Kelvin for input to the thermodynamic calculations of
the rain model.

At upper levels where fewer than 20 stations for the same
area are available for input data, the fields of temperature and dew-
point temperature are much smoother than those at the surface, as would
be expected.

5.3.5 Orographic Precipitation

The analysis of computed precipitation due to orographic ascent

is shown in Figure (5-15) and the verification at 18Z of October 14, 1960 in Figure (5-16). A first inspection of the computed chart would indicate that the calculated rainfall amounts are too high. However, some very interesting features are present, such as the "hole" in the precipitation pattern over south-central British Columbia. Large orographic precipitation amounts are calculated along the West Coast as anticipated, and also substantial amounts along the windward slope of the Alberta Range. Naturally evaluation is difficult along the coastal area as rain associated with the frontal system is also present. All that can be said is that the orographic effect appears to enhance the rainfall which would occur if the terrain were not present. Farther north along the Alaska Panhandle observed amounts are considerably less than those near the Queen Charlotte Islands and are of the same order of magnitude as the computed values. Also Sitka (SIT) reports no precipitation for the previous 6 hours and none is calculated.

The last few statements may seem to indicate that the precipitation over the Alaska Panhandle is largely orographic in origin, but too much should not be read into these comparisons as much more data are needed to substantiate these findings. Another successful predication is the precipitation at Fort Simpson (FS) in the Northwest Territories. No frontal activity can be identified as the likely cause so that the precipitation may be entirely orographic in nature.

Computed trace amounts should be regarded with suspicion as the assumption that no evaporation occurs during the descent is not strictly valid. Another problem which is not treated at all by the rain model is the horizontal advection of raindrops. O'Neill (1966) found that computed maxima were displaced upstream from the observed precip-

itation maxima, but no statement concerning this matter can be made here as observations are far too scarce.

One of the worst failures of the model was a computed value of .05 inches at Pincher Creek (PC), Alberta while the actual 18Z report indicates virtually clear skies and no precipitation over the past 6 hours. The explanation is believed to lie in the assumption that the circulation did not change markedly over the 6-hour period.

The lack of surface observations makes further comparisons difficult. A better evaluation could be attempted by supplementing regular reports with climatological reports and forestry observations in the summer months. However, the above discussion does offer some encouragement that the results may be useful.
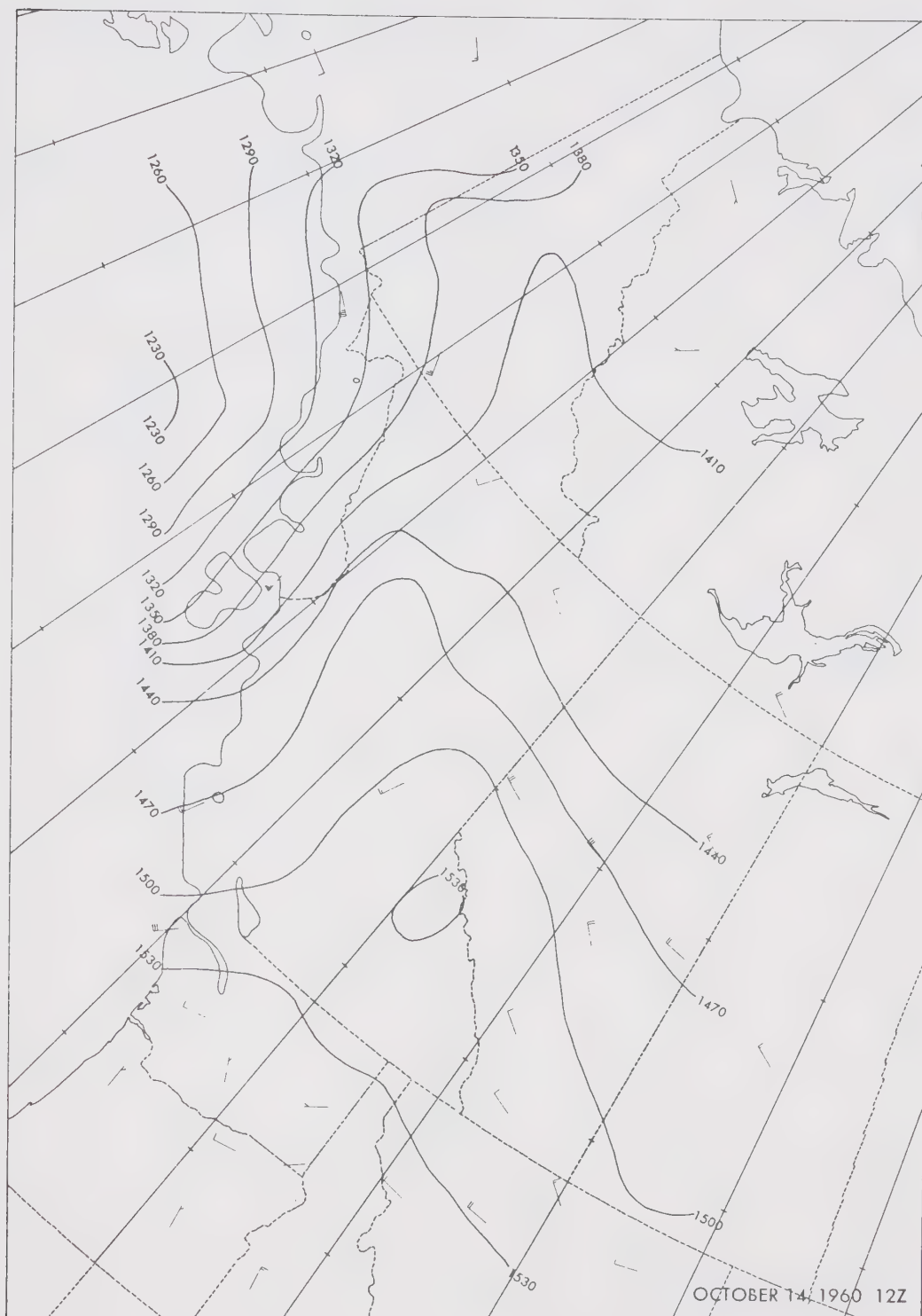
FIGURE (5-8) Modified stream-function analysis at the 850-mb level on
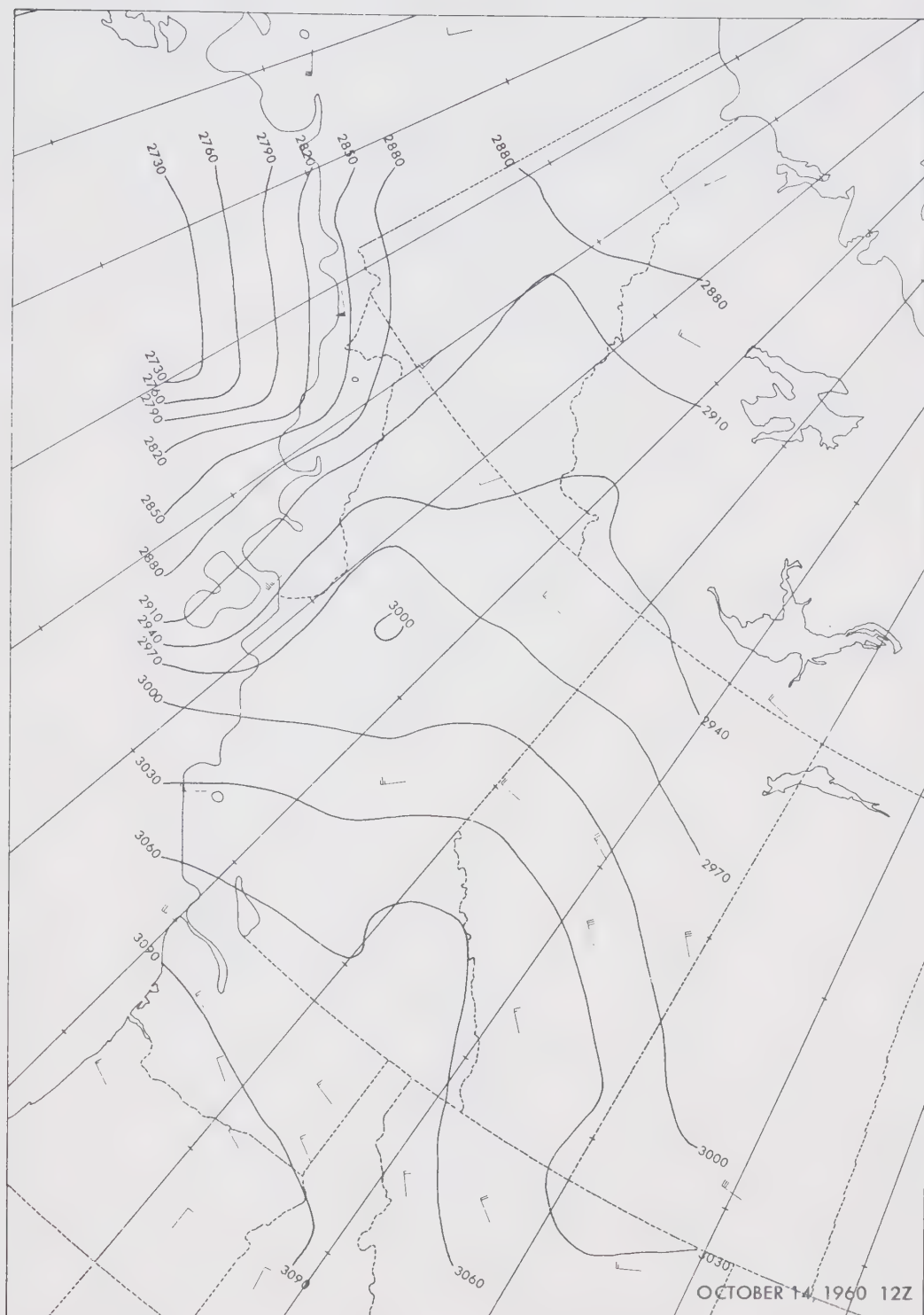October 14, 1960 - 12Z. Contours are drawn at 30-gpm intervals.

FIGURE (5-9) Modified stream-function analysis at the 700-mb level
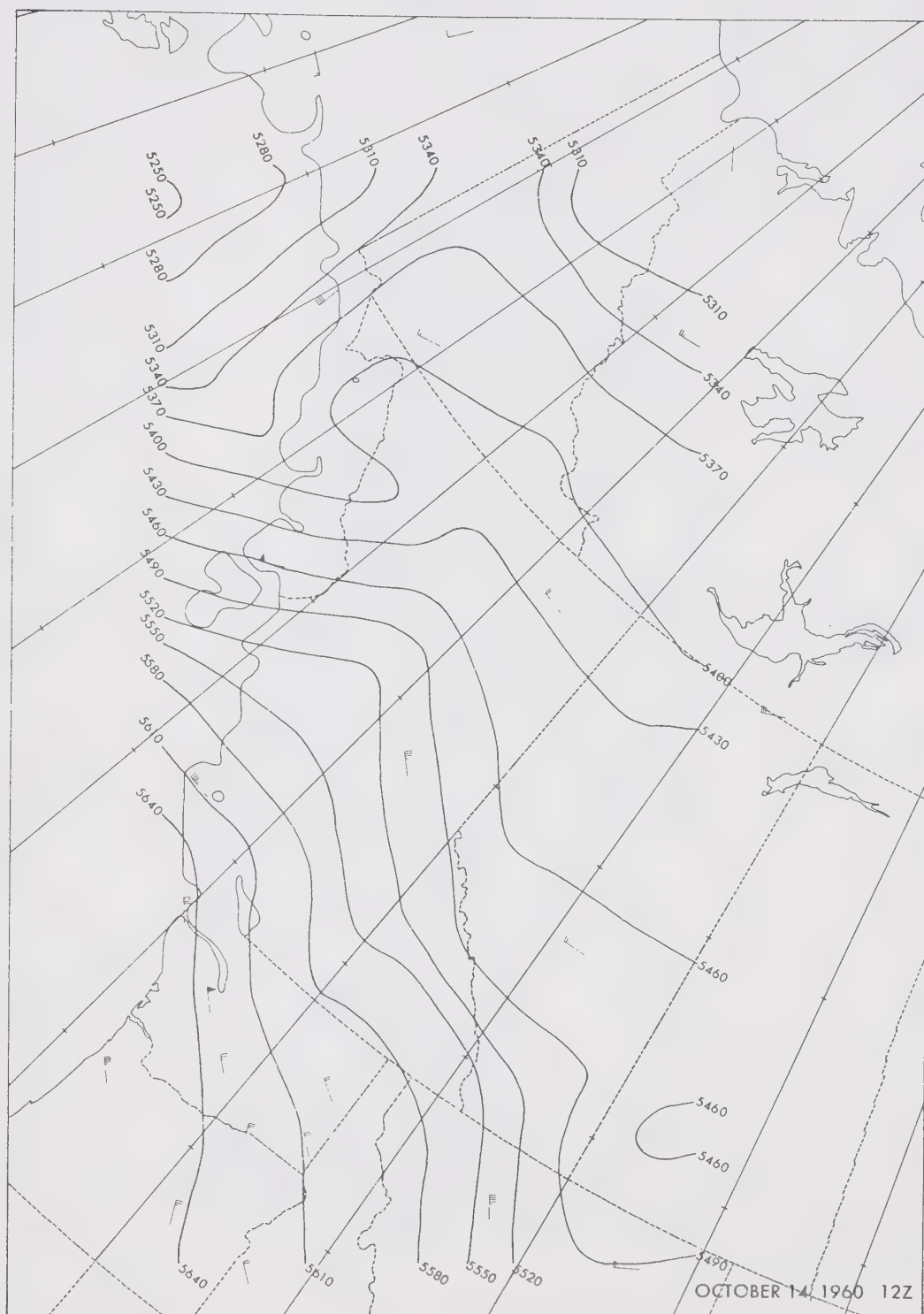on October 14, 1960 - 12Z. Contours drawn at 30-gpm intervals.

FIGURE (5-10) Modified stream-function analysis at the 500-mb level
on October 14, 1960 - 12Z. Contours drawn at 30-gpm intervals.
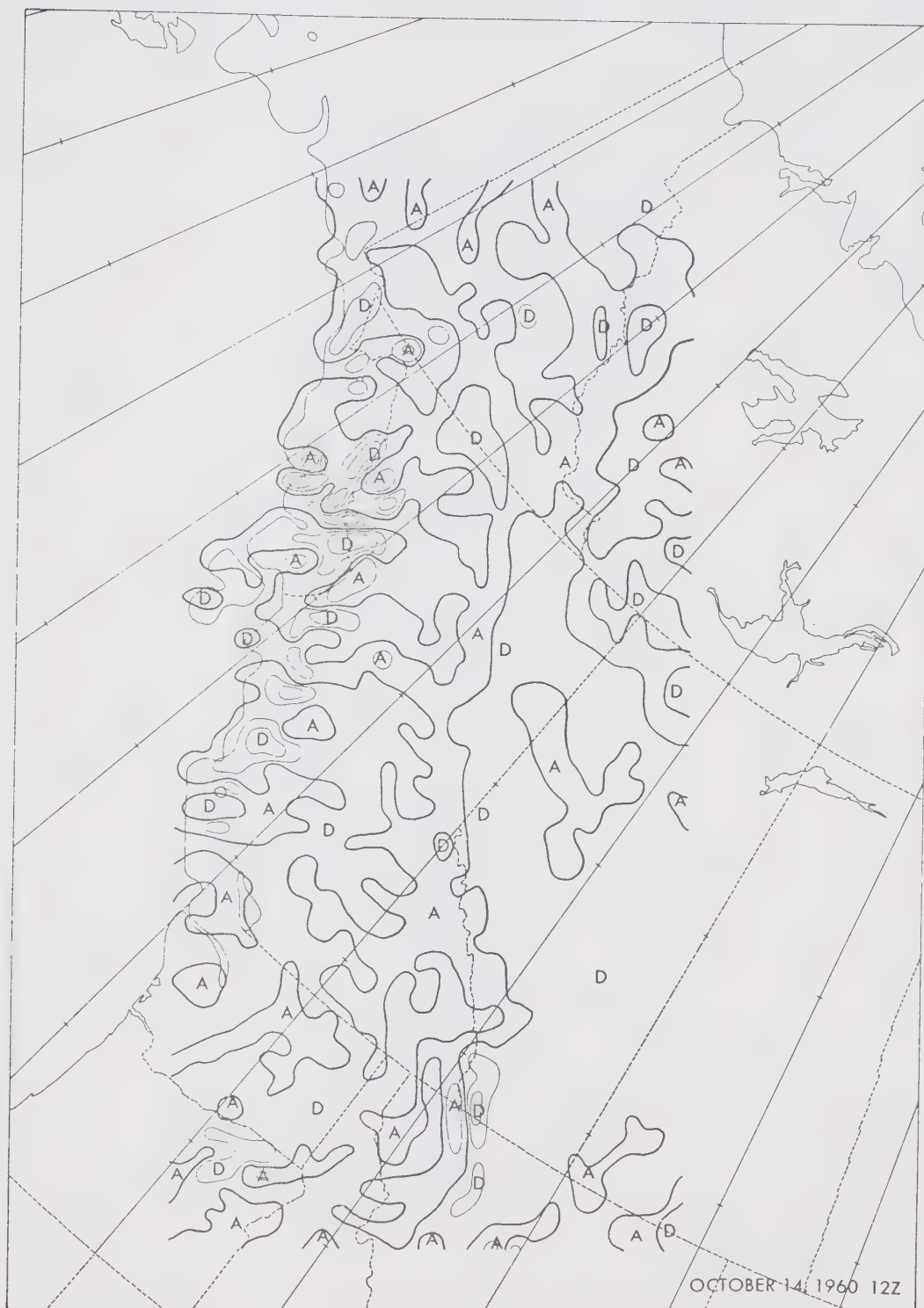
OCTOBER 14, 1960 12Z

FIGURE (5-11) Surface vertical velocity induced by flow over sloping terrain on October 14, 1960 - 12Z. The heavy solid line separates regions of ascending and descending motion. Isotachs are drawn at 5, 10 and 40 cm/sec. The letters A and D represent ascent and descent respectively.
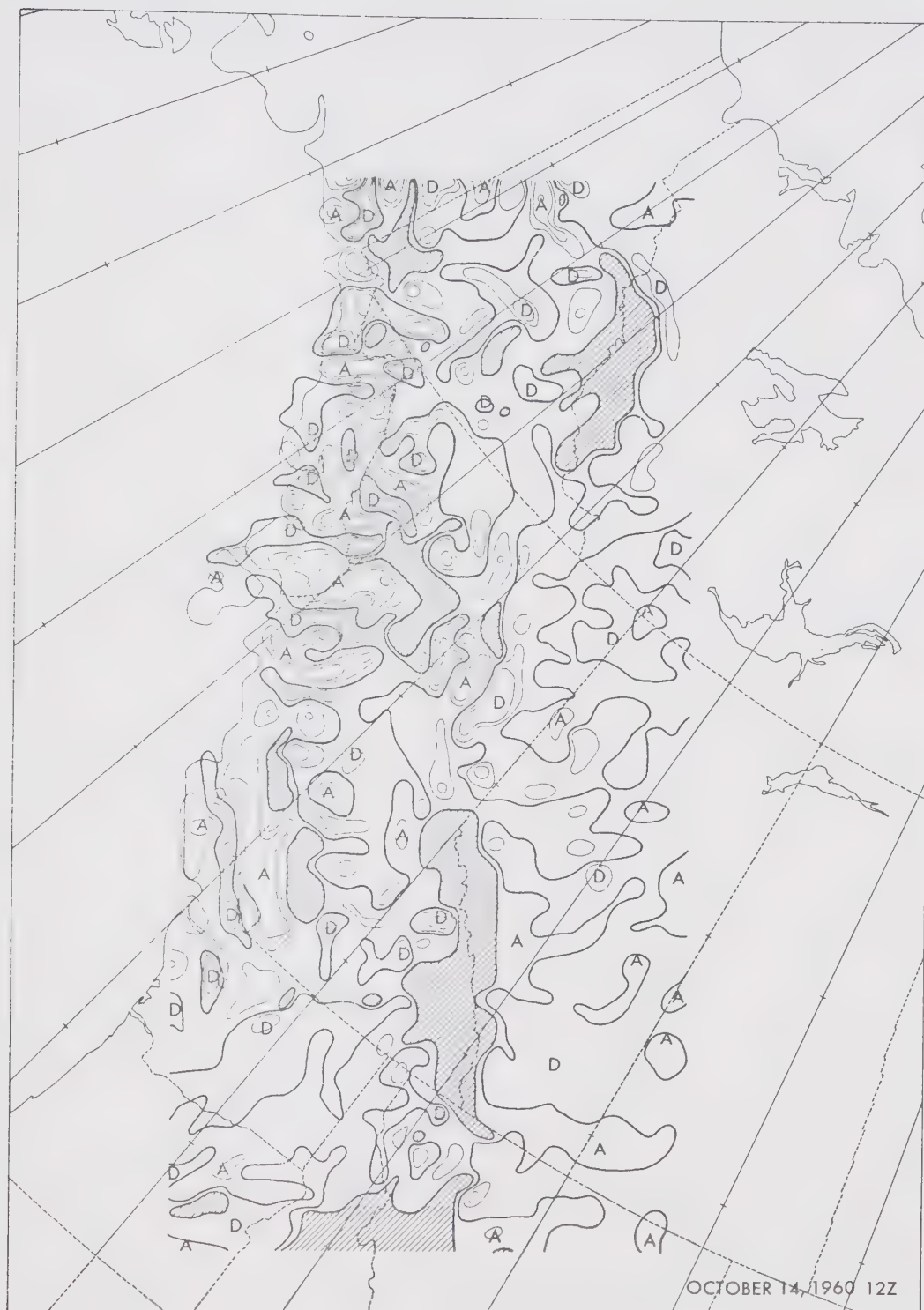
FIGURE (5-12) Terrain-induced vertical velocities at the 850-mb level on October 14, 1960 - 12Z. Ascending and descending motions are marked by the letters A and D respectively and are separated by a heavy solid line. Isotachs at 5, 10 and 40 cm/sec. Shaded areas indicate surface below terrain.
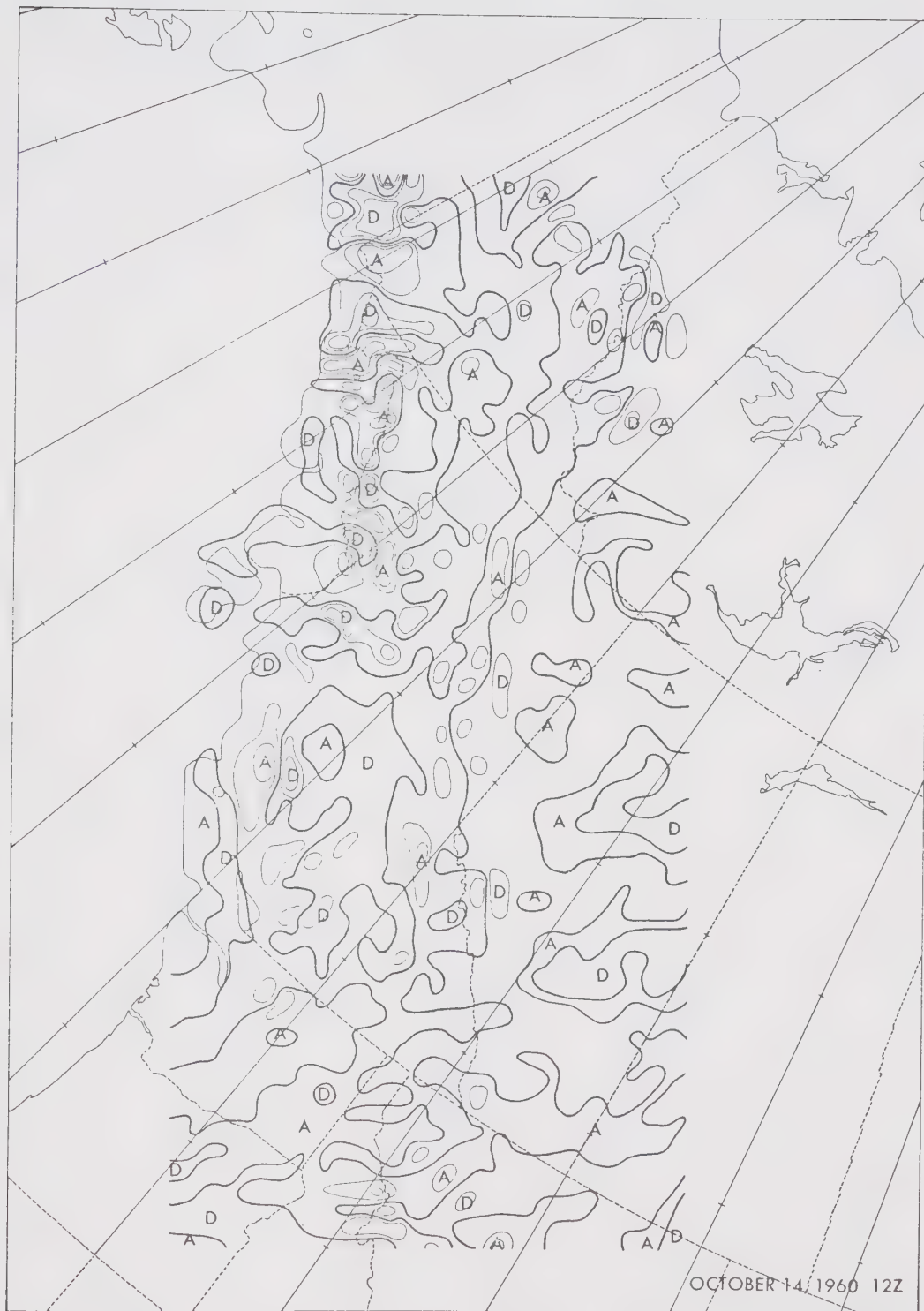
FIGURE (5-13) Terrain-induced vertical velocities at the 700-mb level
on October 14, 1960 - 12Z. Ascent and descent are denoted by the
letters A and D respectively and separated by heavy solid line. Iso-
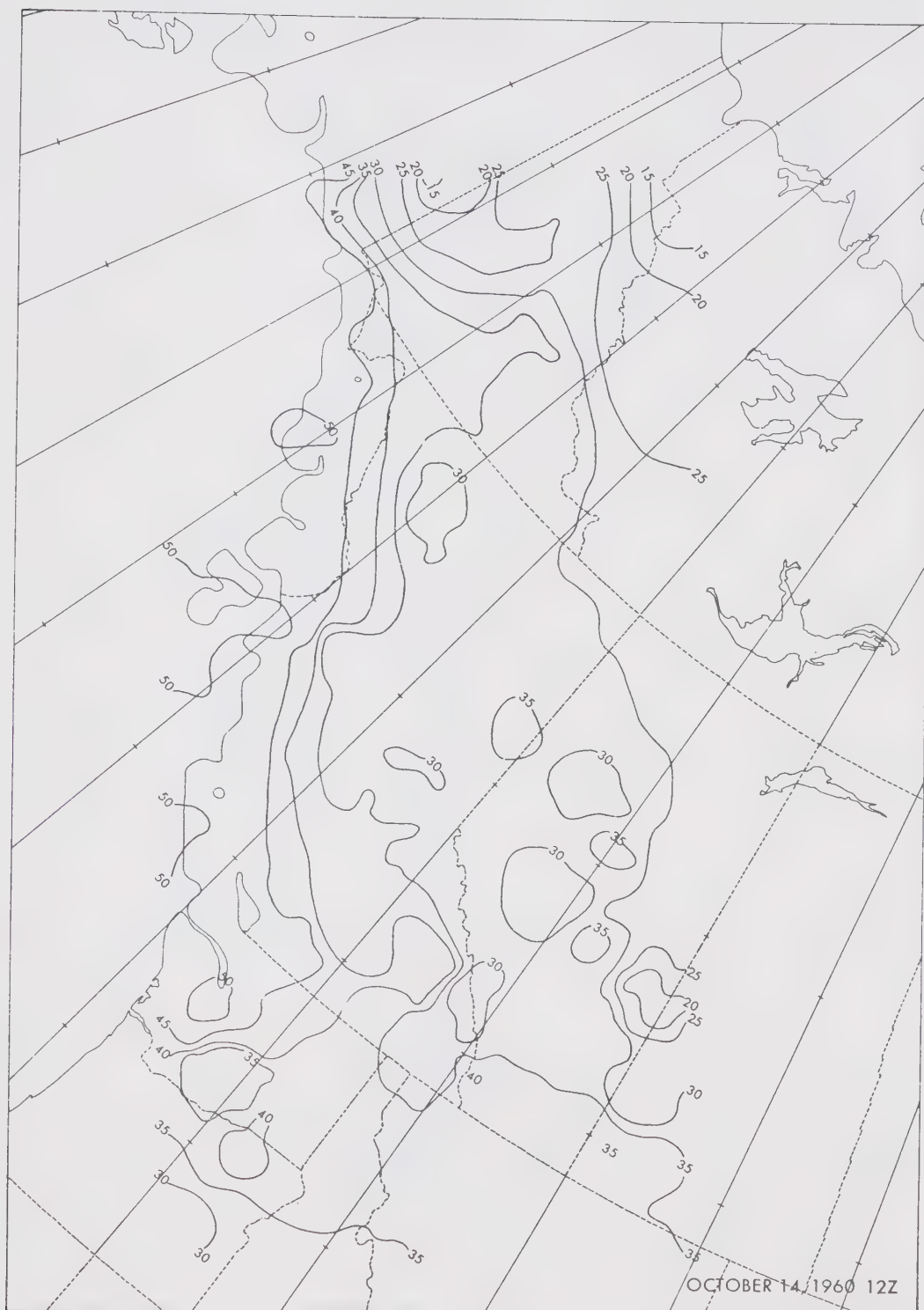tachs at 5, 10 and 40 cm/sec.

FIGURE (5-14) Objective analysis of surface temperature on October 14, 1960 - 12Z. Isotherms are drawn every 5 degrees and temperatures are in Fahrenheit.
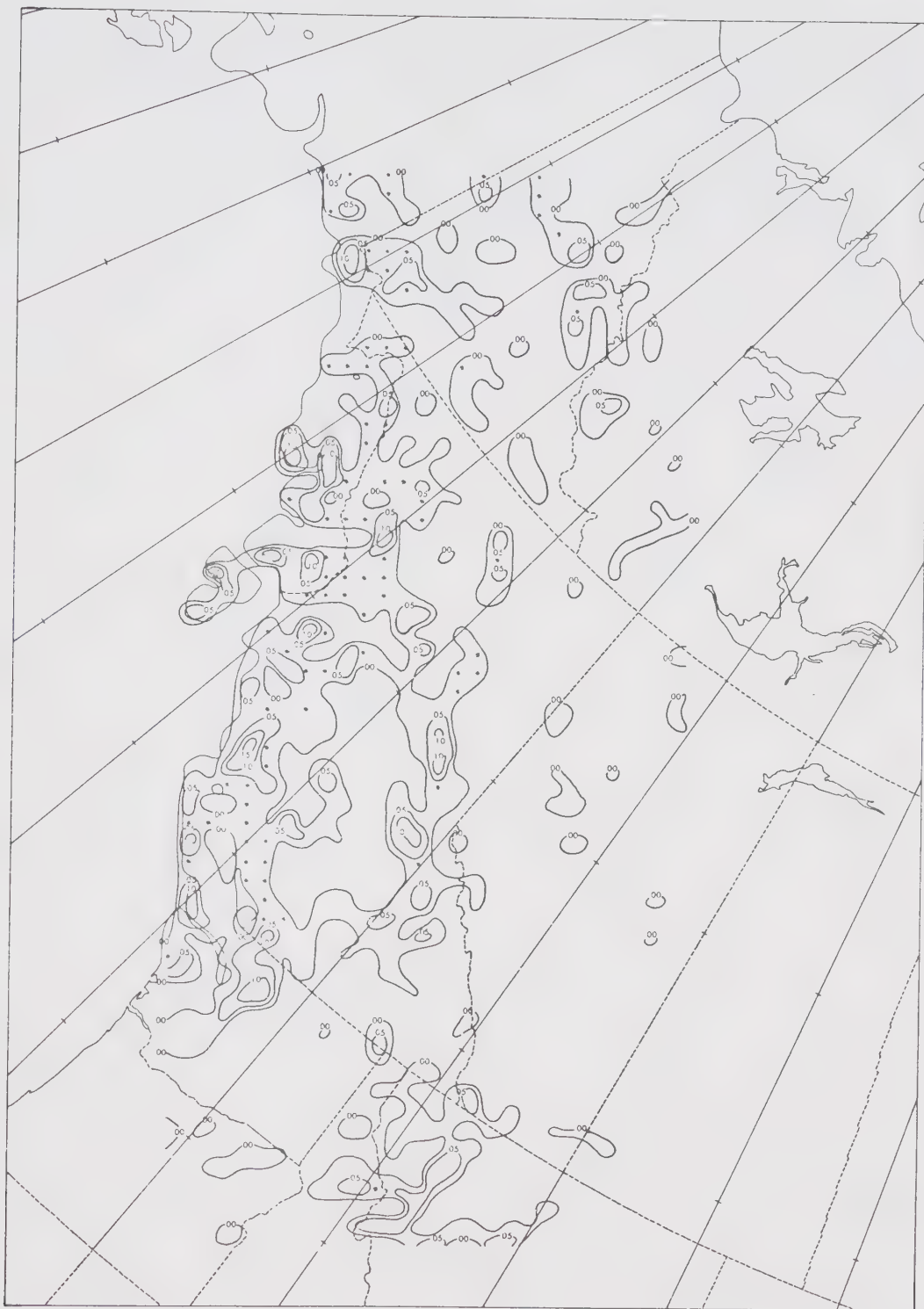
FIGURE (5-15) Analysis of computed rainfall amounts in inches.
Isohyets are drawn at .00 (a trace), .05, .10, and .15 inches. Asterisks
denote ascent greater than 10 cm/sec above the point considered. Values
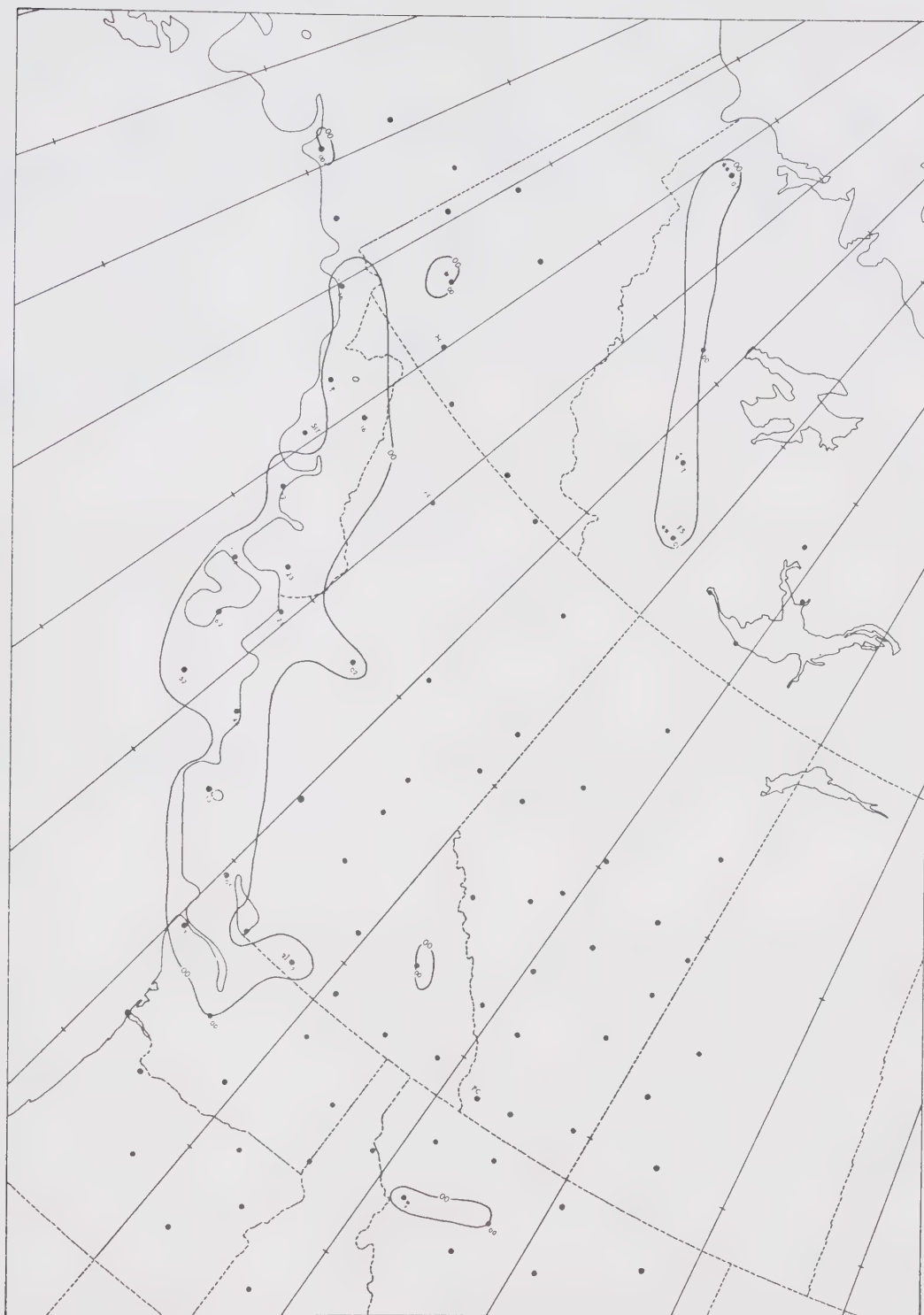are calculated for October 14, 1960 from 12Z to 18Z.

FIGURE (5-16) Observed 6-hour rainfall amounts over past 6 hours on October 14, 1960 - 18Z. Also shown is present weather. Each station used in the analysis is marked by a large dot. The presence of an amount to the lower right of a dot gives a value greater than zero for the precipitation during the previous 6 hours.

5.4   June 21, 1960 - 00Z

5.4.1   The Synoptic Situation

This particular case is chosen to illustrate the point that the Rocky Mountains are partially responsible for much of the precipitation received in Alberta in the spring and early summer months, for, as Reinelt (1970) has pointed out, an easterly circulation for Alberta is just as much an upslope situation as a westerly flow is for the British Columbia coast.

At 00Z, June 19, 1960, a somewhat ill-defined low and an associated frontal wave are situated over southern British Columbia. The associated low at 500 mb is centred near the southern tip of the Queen Charlotte Islands. By the same time on June 20, two surface centres are visible, one south of Edmonton and the other immediately west of Glasgow, Montana. The 500-mb low has now assumed the former position of the surface feature. The temperature at its centre is near -30°C.

By June 21 the Glasgow low has merged with a series of lows which comprise a trough complex extending from Colorado to southeast Saskatchewan, recurving to the low some 100 kilometers north of Edmonton. The cold low is now established almost vertically above this surface position, and the air-mass associated with it is moist and unstable.

The surface low eventually intensified and moved slowly southeast over the next two days, during which time much of Alberta was subjected to a northeasterly flow with its consequent cloud and showers.

5.4.2   The Stream-Function Analyses

All three levels are handled well by the objective stream-

function analysis (see Figures (5-17), (5-18), (5-19)). A peculiar gradient is evident in the upper right corner of the 850-mb analysis but the absence of a reported wind at Inuvik is a likely cause. Also, a direct iterative compromise between Norman Wells and Fairbanks is not possible as they are separated by a distance greater than 600 km.

The only feature not picked up by the subjective height-contour analysis which was recognized by the $\overset{*}{\psi}$ analysis was a minor trough at the 850-mb level as indicated by the wind at Calgary.

5.4.3 Vertical Velocity Fields

The instability of the air mass which covers the southern half of Alberta is the reason for much of the precipitation observed in this area. However, the most persistent region of rainfall is observed over the Peace River area and south to Jasper. With reference to vertical velocity charts, Figures (5-20) to (5-22), this same region is marked by substantial orographic ascent at all three levels. The position of the low makes it impossible for ascent to occur along the entire eastern slope of the Alberta Range. In fact, an area of descent is observed to extend almost unbroken from Edson south where a return westerly flow exists.

In this instance, the rain is not solely an orographic phen-omenon but, doubtless, terrain-induced vertical motions play an import-ant role. Just exactly what this role may be is masked by the presence of convective precipitation. The rain model is not capable of handling instability cases so that it was not applied to this situation.
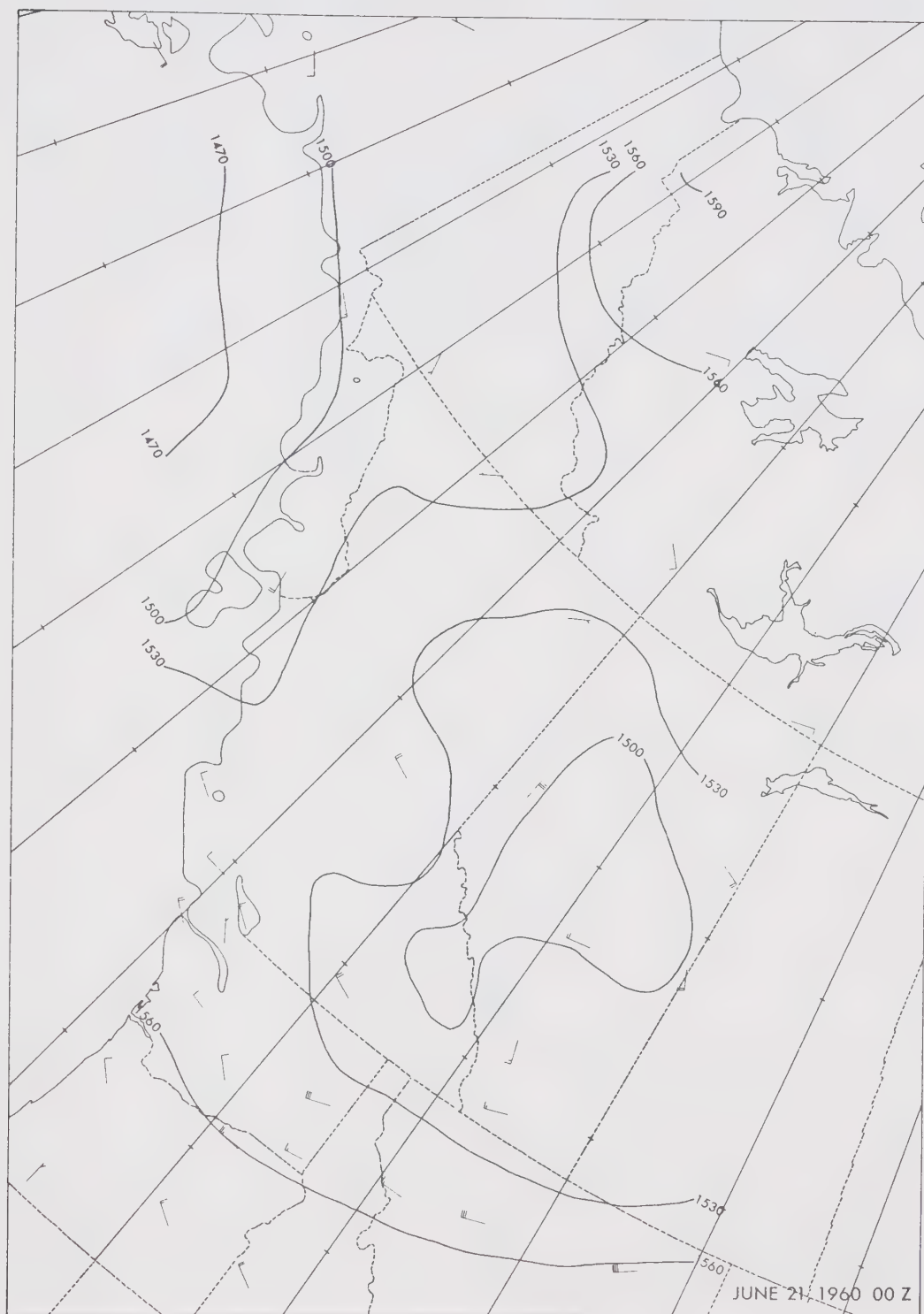
FIGURE (5-17) Modified stream-function analysis at 850-mb level on June 21, 1960 - 00Z. Contours drawn at 30-gpm intervals.
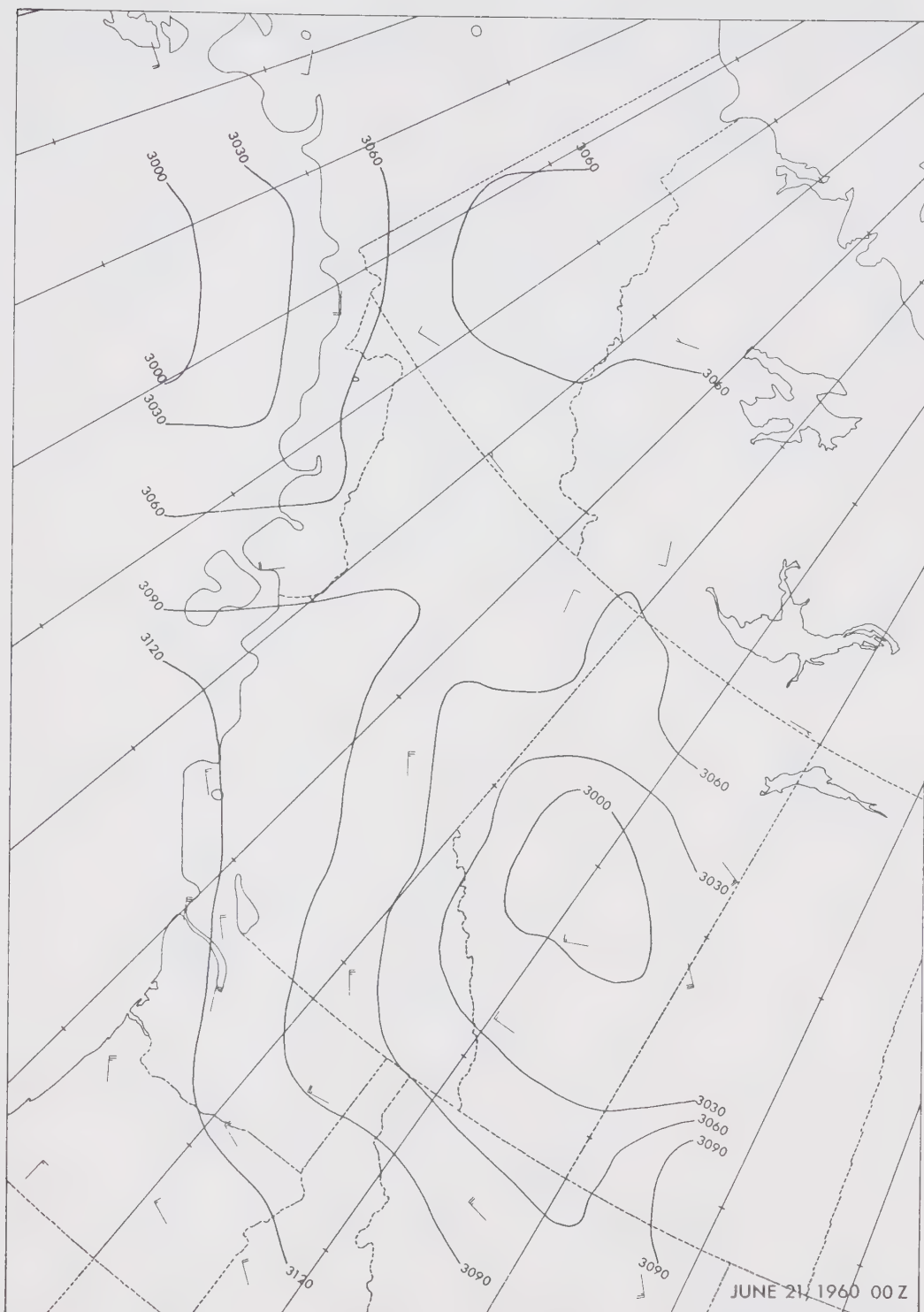
FIGURE (5-18) Modified stream-function analysis at the 700-mb level
on June 21, 1960 - 00Z. Contours drawn at 30-gpm intervals.

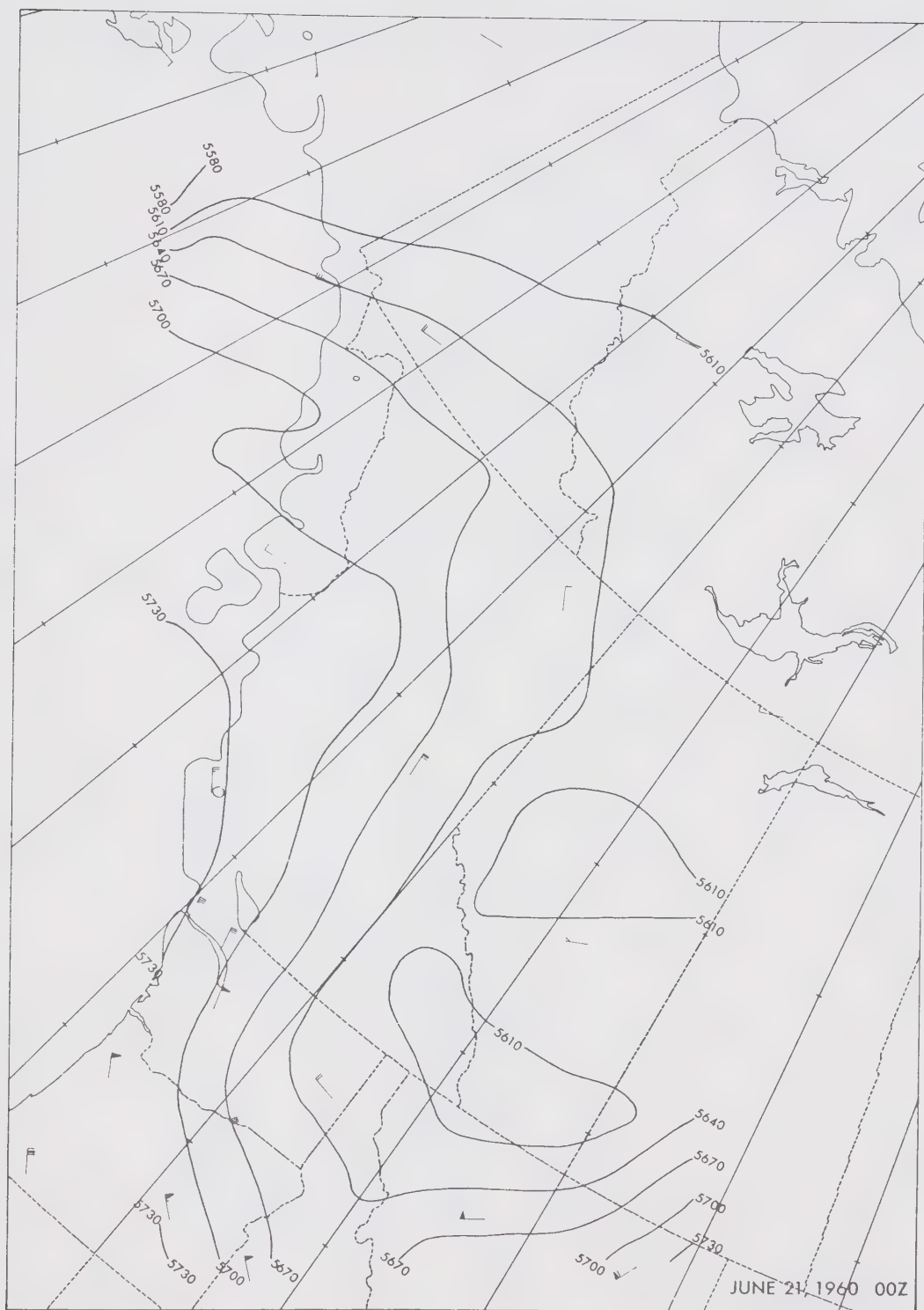FIGURE (5-19) Modified stream-function analysis at the 500-mb level on June 21, 1960 - 00Z. Contours drawn at 30-gpm intervals.
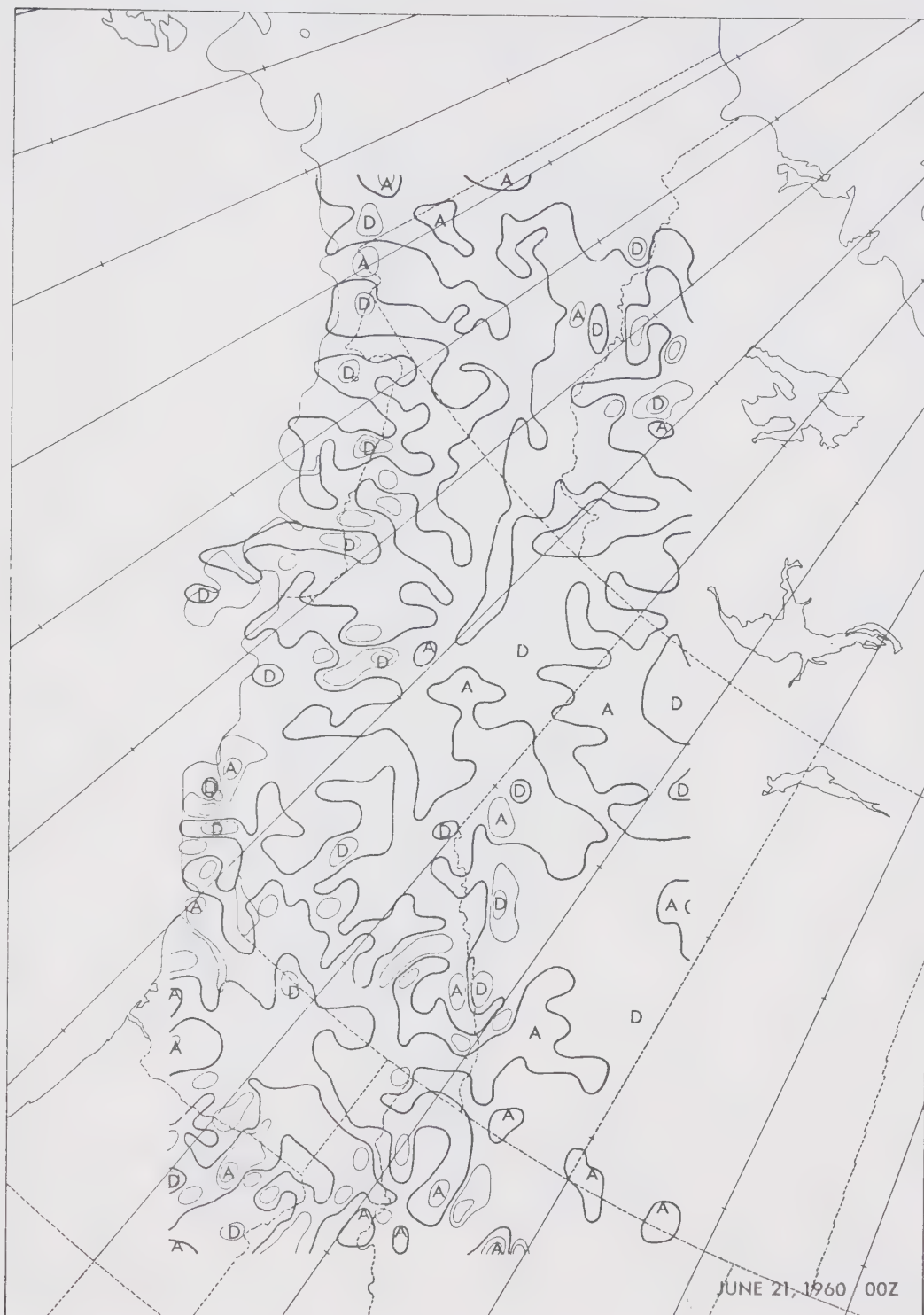
FIGURE (5-20) Surface vertical velocity induced by flow over sloping
terrain on June 21, 1960 - 00Z. The heavy solid line separates
regions of ascending and descending motion. Isotachs are drawn at 5,
10 and 40 cm/sec. The letters A and D represent ascent and descent
respectively.

FIGURE (5-21) Terrain-induced vertical velocities at the 850-mb level on June 21, 1960 - 00Z. Ascending and descending motions are marked by the letters A and D respectively and are separated by a heavy solid line. Isotachs at 5, 10 and 40 cm/sec. Shaded areas indicate that this level is below the terrain.

FIGURE (5-22) Terrain-induced vertical velocities at the 700-mb level
on June 21, 1960 - 00Z. Ascent and descent are denoted by the letters
A and D respectively and separated by heavy solid line. Isotachs at
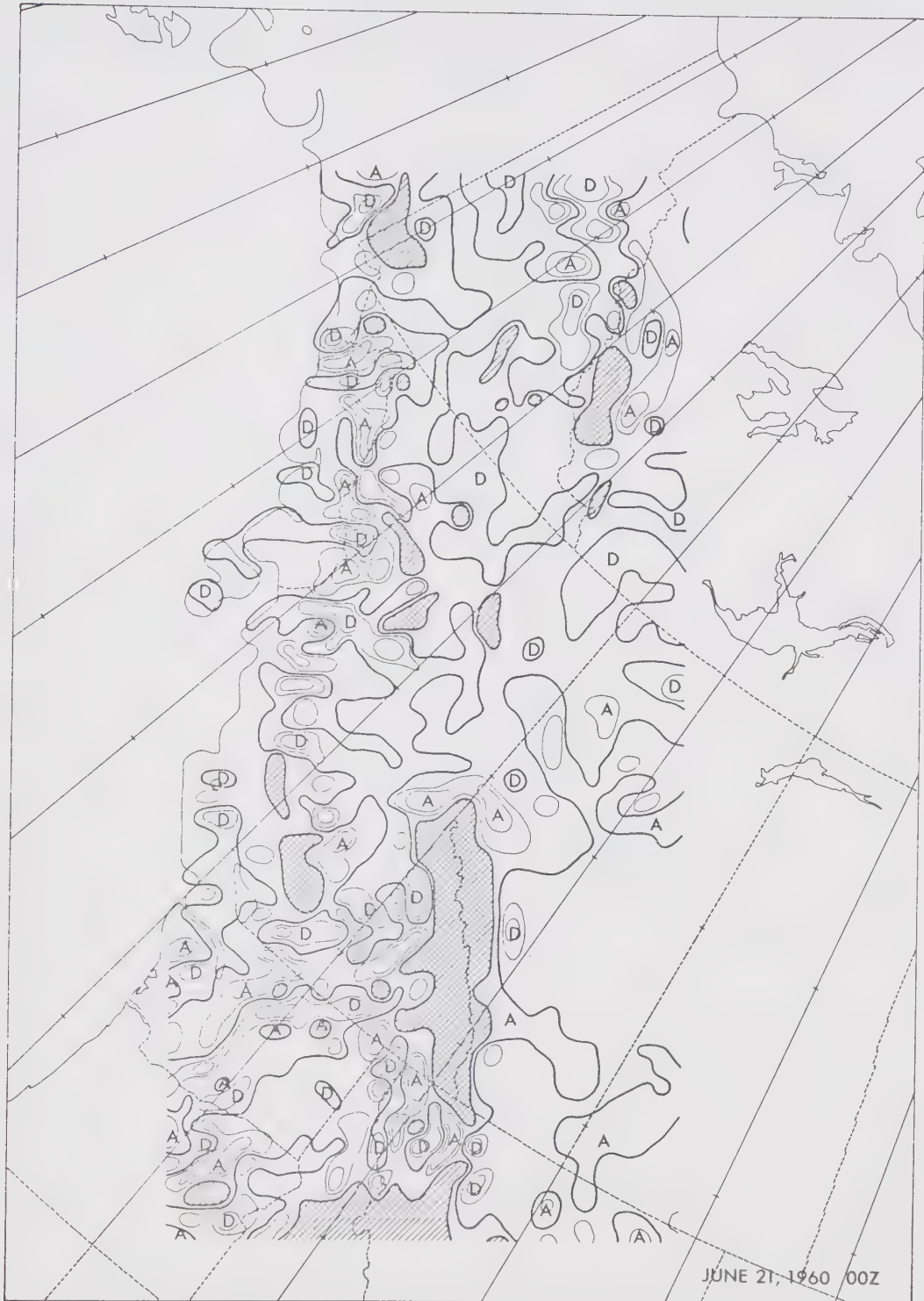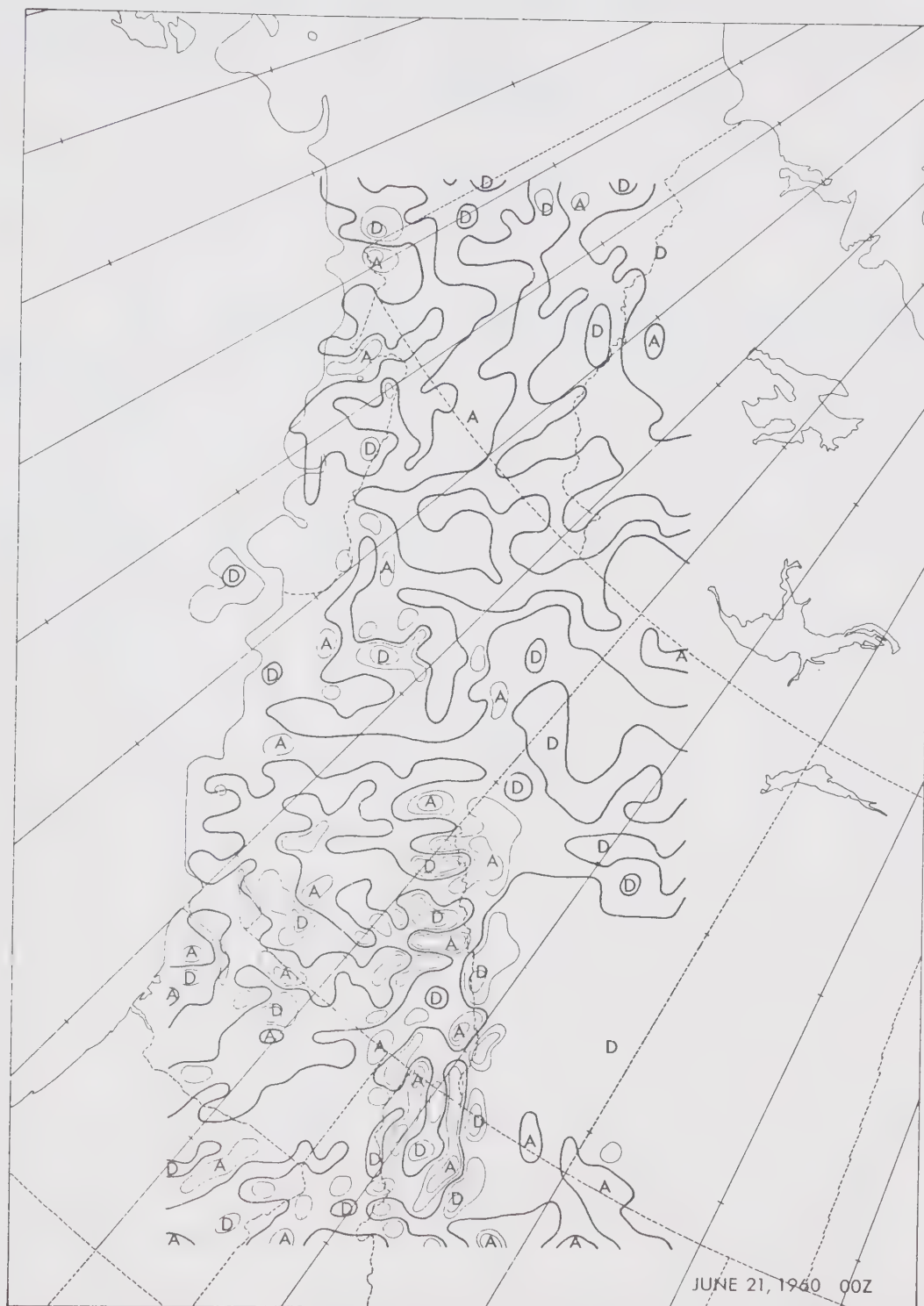5, 10 and 40 cm/sec.

CHAPTER 6

CONCLUSIONS

The iterative procedure for calculating the modified stream-
function has been improved to the point that far fewer station reports
are required to arrive at a reasonable field. After considerable exper-
imentation with Charette's (1971) model, this approach was found neces-
sary because a great deal of time was spent subjectively interpolating
winds and heights at the particular pressure level under examination from
charts already subjectively analyzed by hand. This amounted to placing
a great deal of faith in the geostrophic relation. Therefore, it was
decided to revert to Endlich and Mancuso's original stream-function
calculation which was based solely on the reported winds. The reported
heights at radiosonde stations were used only as an initial guess for
the modified stream-function in order that the final field had values
closely approximating the heights at the constant pressure level.

This approach proved reasonably satisfactory. The regular
radiosonde reports supplemented by pilot balloon reports were sufficient
to determine the flow over the continent. Because of the lack of ade-
quate data networks this is not possible over the oceans so that this
procedure is restricted primarily to the land areas. Emphasis should
be placed on the need for the supplementary reports, particularly in
northern British Columbia and the central Yukon. As is illustrated
in the 00Z, October 14, 1960 situation, some unusually strong gradients

may arise when the distance between stations is large and the inter-vening pattern not uniform.

The continuous weighting scheme introduced here, while only slightly less arbitrary, substantially simplifies the computer pro-gramming and reduces the storage required. It also has the advantage that minor peculiarities may be maintained in those regions where data are dense, while providing a reasonably smooth interpolation in data-sparse areas.

The final stream-function objective analysis provides a useful tool and could easily be adapted to a small computer facility. An error rejection scheme would have to be formulated for direct input of information from teletype. In this study, analysis was restricted to the standard levels of synoptic analysis, but operationally it could be applied to any level where reasonable data density exists.

Little change was made to the method of computing orographic vertical velocities proposed by Charette. The use of the extracted terrain heights at one-eighth grid length intervals combined with the reduction of the finite difference increment for calculation of terrain slopes complicated the pattern of orographic vertical motion. It is difficult to assess whether this yields any significant improvement or merely confuses the issue. Because of friction, vertical velocities at the surface are likely to be underestimates, while at the 850-mb and 700-mb surfaces the estimates may be too high. Daily evaluation is required to reveal systematic errors so that a more realistic decrease of the orographic influence with height may be formulated.

A precipitation model similar to the one suggested in Chapter 4 is useful in the evaluation of ascending motion but provides no prac-

tical estimate of the magnitude of downward motion. Charette's treatment of valleys and peaks may provide a better method for narrow valleys, but to the lee of major topographic features would tend to underestimate negative vertical velocity. The current procedure is probably better in the latter case, provided one realizes that minor centres of descent over frequently fluctuating topography are not likely present, due to stagnation of air in valleys.

As suggested in Chapter 5, a finer network of rain gauges is required to evaluate the orographic precipitation. Climatological and forestry reports would be invaluable as well.

BIBLIOGRAPHY

Brunt, D., 1933: The Adiabatic Lapse-Rate for Dry and Saturated Air. Quart. J. Roy. Meteor. Soc., 59, 351-360.

Charette, C. D., 1971: Streamline Patterns and Terrain-Induced Vertical Velocities in the Canadian Cordillera. Unpublished M.Sc.Thesis, Dept. of Geography, University of Alberta, 117 pp.

Chung, Y. S., 1972: Cyclogenesis in the Lee of the Canadian Rocky Mountains. Unpublished M.Sc. Thesis, Dept. of Geography, University of Alberta, 156 pp.

Cressman, G., 1959: An Operational Objective Analysis System. Mon. Wea. Rev., 87, 367-374.

Endlich, R. and R. Mancuso, 1964: A Direct Method of Stream-Function Computation. Tellus, 16, 32-39.

_____, 1965: An Objective Analysis of Clear Air Turbulence. Stanford Research Institute, Menlo Park, California, Contract Cwb - 10871, 56 pp.

Estoque, M. A., 1957: A Graphically Integrable Prediction Model Incorporating Orographic Influences. J. Meteor., 14, 293-296.

Fukuta, N. and L. A. Walter, 1970: Kinematics of Hydrometeor Growth From a Vapor-Spherical Model. J. Atmos. Sci., 27, 1160-1172.

Fulks, J. R., 1935: Rate of Precipitation From Adiabatically Ascending Air. Mon. Wea. Rev., 291-294.

Haltiner, G. J., 1971: Numerical Weather Prediction. New York, John Wiley and Sons, 317 pp.

Hess, S. L., 1959: Introduction to Theoretical Meteorology. New York, Holt, Rinehart, and Winston, 362 pp.

Hess, S. L. and H. Wagner, 1948: Atmospheric Waves in the Northwestern United States. J. Meteor., 5, 1-19.

Mason, B. J., 1962: Clouds, Rain, and Rainmaking. London, Cambridge University Press, 145 pp.

McClain, E. P., 1960: Some Effects of the Western Cordillera of North America on Cyclonic Activity. J. Meteor., 17, 104-115.

Newton, C. W., 1971: Mountain Torques in the Global Angular Momentum Balance. J. Atmos. Sci., 28, 623-628.

O'Neill, H. R., 1966: Vertical Motion and Precipitation Computations. J. Appl. Meteor., 5, 595-605.

Pettersen, S., 1956a: Weather Analysis and Forecasting. New York, McGraw-Hill Book Co., Vol. 1, 2nd ed., 428 pp.

_____, 1956b: Weather Analysis and Forecasting. New York, McGraw-Hill Book Co., Vol. 2, 2nd ed., 266 pp.

Reinelt, E. R., 1970: On the Role of Orography in the Precipitation Regime of Alberta. The Albertan Geographer, 6, 45-58.

Saucier, W. J., 1955: Principles of Meteorological Analysis, Chicago, University of Chicago Press, 438 pp.

Sawyer, J. S., 1956: The Physical and Dynamic Problems of Orographic Rain. Weather, 11, 375-381.

Smagorinski, J. and G. Collins, 1955: On the Numerical Prediction of Precipitation. Mon. Wea. Rev., 83, 53-68.

Whitaker, S., 1968: Introduction to Fluid Mechanics. Englewood Cliffs, N.Y., Prentice-Hall Inc., 457 pp.

APPENDIX A

Calculation of Wind Direction With Respect to the Grid

$$\theta = (180° - \lambda) + (180° - D) - 10°$$

FIGURE (A-1) Angle the locally measured wind makes with the x-axis of the grid.

With reference to Figure (A-1), it may be seen that the wind direction with respect to the grid depends on the local wind direction D, which is measured relative to true north, the longitude λ where the wind is observed, and the orientation of the grid. The grid is rotated $10°$ so that the ordinate is parallel to $80°W$ and the abscissa to $10°E$. Therefore, once the wind direction is determined with respect to

the zero meridian, subtraction of ten degrees yields the wind direction with respect to the abscissa of the grid.

The angle the wind makes with the local meridian is $180^\circ - D$ while the supplement of the longitude is $180^\circ - \lambda$.

The direction of the wind relative to the x-axis of the grid is:

$$(180^\circ - D) + (180^\circ - \lambda) - 10^\circ = 350^\circ - D - \lambda, \qquad \text{(A-1)}$$

from which the wind components may be calculated.